Journal of Computational Physics: X 3 (2019) 100031

Contents lists available at ScienceDirect

Journal of Computational Physics: X

www.elsevier.com/locate/jcpx

Positivity-preserving, energy stable numerical schemes for the Cahn-Hilliard equation with logarithmic potential

Wenbin Chen [a], Cheng Wang [b,*], Xiaoming Wang [c,d,e,**], Steven M. Wise [f]

[a] Shanghai Key Laboratory for Contemporary Applied Mathematics, School of Mathematical Sciences, Fudan University, Shanghai, 200433, China
[b] Mathematics Department, University of Massachusetts, North Dartmouth, MA 02747, USA
[c] Department of Mathematics, Southern University of Science and Technology, Shenzhen, 518055, China
[d] Fudan University, Shanghai, 200433, China
[e] Florida State University, Tallahassee, FL 32306, USA
[f] Mathematics Department, University of Tennessee, Knoxville, TN 37996, USA

ARTICLE INFO

Article history:
Received 14 October 2018
Received in revised form 14 March 2019
Accepted 30 April 2019
Available online 10 May 2019

Keywords:
Cahn-Hilliard equation
Logarithmic Flory Huggins energy potential
Positivity preserving
Energy stability
Second order BDF scheme
Optimal rate convergence analysis

ABSTRACT

In this paper we present and analyze finite difference numerical schemes for the Cahn-Hilliard equation with a logarithmic Flory Huggins energy potential. Both first and second order accurate temporal algorithms are considered. In the first order scheme, we treat the nonlinear logarithmic terms and the surface diffusion term implicitly, and update the linear expansive term and the mobility explicitly. We provide a theoretical justification that this numerical algorithm has a unique solution, such that the positivity is always preserved for the logarithmic arguments, i.e., the phase variable is always between -1 and 1, at a point-wise level. In particular, our analysis reveals a subtle fact: the singular nature of the logarithmic term around the values of -1 and 1 prevents the numerical solution reaching these singular values, so that the numerical scheme is always well-defined as long as the numerical solution stays similarly bounded at the previous time step. Furthermore, an unconditional energy stability of the numerical scheme is derived, without any restriction for the time step size. Such an analysis technique can also be applied to a second order numerical scheme in which the BDF temporal stencil is applied, the expansive term is updated by a second order Adams-Bashforth explicit extrapolation formula, and an artificial Douglas-Dupont regularization term is added to ensure the energy dissipativity. The unique solvability and the positivity-preserving property for the second order scheme are proved using similar ideas, namely, the singular nature of the logarithmic term plays an essential role. For both the first and second order accurate schemes, we are able to derive an optimal rate convergence analysis. The case with a non-constant mobility is analyzed as well. We also describe a practical and efficient multigrid solver for the proposed numerical schemes, and present some numerical results, which demonstrate the robustness of the numerical schemes.

* The first corresponding author.
** The second corresponding author.
E-mail addresses: wbchen@fudan.edu.cn (W. Chen), cwang1@umassd.edu (C. Wang), wxm@math.fsu.edu (X. Wang), swise1@utk.edu (S.M. Wise).

https://doi.org/10.1016/j.jcpx.2019.100031

1. Introduction

The well-known Allen-Cahn (AC) [3] and Cahn-Hilliard (CH) [16] equations are prototypical gradient flows with respect to a given free energy. We consider a bounded domain $\Omega \subset \mathbb{R}^d$ (with $d = 2$ or $d = 3$). For any $\phi \in H^1(\Omega)$, with a point-wise bound, $-1 < \phi < 1$, the energy functional is given by

$$E(\phi) = \int_\Omega \left((1+\phi)\ln(1+\phi) + (1-\phi)\ln(1-\phi) - \frac{\theta_0}{2}\phi^2 + \frac{\varepsilon^2}{2}|\nabla\phi|^2 \right) d\mathbf{x}, \tag{1}$$

where ε, θ_0 are positive constants associated with the diffuse interface width. See [15,24,30,32]. The AC and CH equations are weighted L^2 (non-conserved) and H^{-1} (conserved) gradient flows of the energy functional (1), respectively,

$$\partial_t \phi = -\mathcal{M}(\phi)\mu, \qquad \text{(Allen-Cahn)} \tag{2}$$

and

$$\partial_t \phi = \nabla \cdot (\mathcal{M}(\phi)\nabla\mu), \qquad \text{(Cahn-Hilliard)} \tag{3}$$

where μ is the chemical potential

$$\mu := \delta_\phi E = \ln(1+\phi) - \ln(1-\phi) - \theta_0\phi - \varepsilon^2\Delta\phi, \tag{4}$$

and $\mathcal{M}(\phi) > 0$ is the mobility function. In a related example, Cahn et al. [15] have studied the Cahn-Hilliard equation with the fully degenerate mobility, $\mathcal{M}(\phi) = (1-\phi)(1+\phi)$, and have shown asymptotic convergence to a geometric model for motion by the surface Laplacian of mean curvature. In this article we focus on the more challenging Cahn-Hilliard model; the extensions to the Allen-Cahn part is straightforward, and we present a simple case in Appendix A.

For simplicity of presentation, we suppose Ω is a cuboid and consider periodic boundary conditions. The case with homogeneous Neumann boundary conditions can be analyzed in a manner similar to that used here. Due to the gradient structure of (3), the following energy dissipation laws formally hold:

$$\frac{d}{dt}E(\phi(t)) = -\int_\Omega \mathcal{M}(\phi)|\nabla\mu|^2 d\mathbf{x} \le 0. \tag{5}$$

The free energy with the logarithmic potential is often considered to be more physically realistic than that with a polynomial free energy, because the former can be derived from regular or ideal solution theories [30]. However, one well-known difficulty for the analysis of these models with logarithmic Flory Huggins energy potential – as it is called in the polymer science community [30] – is associated with the singularity as the phase variable approaches -1 or 1. PDE solutions are expected to satisfy a *positivity property*, specifically,

$$0 < 1-\phi \quad \text{and} \quad 0 < 1+\phi. \tag{6}$$

In other words, the phase variable remains in the interval $(-1, 1)$, in a point-wise sense [32]. However, it is a major challenge to create numerical schemes that mimic this property. To avoid such a subtle challenge, many efforts have been devoted to a polynomial approximation:

$$E(\phi) = \int_\Omega \left(\frac{1}{4}(\phi^2-1)^2 + \frac{\varepsilon^2}{2}|\nabla\phi|^2 \right) d\mathbf{x}, \tag{7}$$

which leads to the nonlinear, but non-singular, chemical potential

$$\mu := \delta_\phi E = \phi^3 - \phi - \varepsilon^2\Delta\phi. \tag{8}$$

This model has a similar double-well structure as in the case (1) and (4), but avoids the singularities as the phase variable approaches -1 or 1. Meanwhile, the PDE solution may go beyond the given interval of $(-1, 1)$. There have been extensive numerical works for the Cahn-Hilliard equation with the polynomial approximation (7), (8); see the related references [23, 31,33,37,43,49,50,65], etc.

In this article we study the Cahn-Hilliard model with logarithmic Flory Huggins energy potential (1). At the PDE level, the positivity property (for both logarithmic arguments, $1+\phi$ and $1-\phi$) has been established in [2,26,32,55]. Moreover, in the 1-D and 2-D cases, the phase separation has also been justified at a theoretical level, i.e., a uniform distance between the phase variable and the singular limit values (-1 and 1) have been derived, dependent on ε, θ_0 and the initial data. The analysis for the degenerate mobility case could be found in [8,32]. In addition, an improved analysis for the 2-D equation has been reported in a more recent work [38]; also see the related references [22,54]. An extension to the Cahn-Hilliard model coupled with fluid flow is also discussed in [1,39].

At the level of numerical scheme design, the positivity preserving property is very challenging, due to the particularities of the spatial and temporal discretizations involved. There have been extensive numerical works for the CH model with Flory Huggins energy potential [35,47,48,51,52,56–58,67], while a theoretical justification to assure the positivity of $1+\phi$ and $1-\phi$ has not been available (so that the numerical scheme is unconditionally well-defined). Among the existing literature, it is worth mentioning the numerical analysis to theoretically justify this issue in [24]. The authors analyzed the implicit Euler scheme applied to the CH equation (3), (4), combined with the finite element approximation in space. In more details, the following result was proved: *Under the condition that* $\Delta t \le \frac{4\varepsilon^2}{\theta_0^2}$, *and the initial data satisfy* $\frac{1}{|\Omega|}\left|\int_\Omega \phi_0(\mathbf{x})\,d\mathbf{x}\right| < 1-\delta$, $\|\phi_0\|_\infty \le 1$, *then there is a unique numerical solution for the fully implicit Euler scheme, satisfying* $\|\phi^n\|_\infty < 1$. An extension to the multi-component Cahn-Hilliard flow has also been reported in [12].

Meanwhile, it is observed that, an energy stability property is not unconditionally available for the scheme studied in [24], due to the implicit treatment of the concave diffusion term. Further, the time step constraint, $\Delta t \le \frac{4\varepsilon^2}{\theta_0^2}$, could make the numerical implementation challenging for small ε and large θ_0. In this article, we propose and analyze an alternate numerical scheme, in which the implicit treatment for the concave diffusion term is replaced by an explicit one, combined with centered difference discretization in space. Again, the implicit treatment for the nonlinear logarithmic term requires a theoretical justification for the positivity of both $1+\phi$ and $1-\phi$, so that the numerical scheme is well-defined at a point-wise level. Instead of reconstructing an alternate energy functional to avoid the singularity for ϕ at -1 and 1, as reported in [12,24], we use a new technique to theoretically justify the positivity of the numerical solution. First, the fully discrete numerical scheme corresponds to a minimization of a discrete energy function. And also, such an energy functional is strictly convex, as long as the phase variable stays within $(-1,1)$ at a point-wise level. Subsequently, to avoid a circular "chicken-and-the-egg" argument, we take a closed domain for the numerical solution variables, in which the limit bound values of -1 and 1 are not reachable. In turn, the continuous energy function has to have a global minimum over this closed domain. Moreover, we make use of the following subtle fact: the singular nature of the logarithmic function prevents such a global minimum from being obtained at a boundary point (in terms of numerical solution variable domain), as long as the numerical solution stays bounded at the previous time step. As a result, since the global minimum could only possibly occur at an interior point in the numerical solution variable domain, we conclude that the numerical scheme has to be satisfied, so that the existence of the numerical solution is proved. In addition, due to the convex nature of the energy function, the uniqueness of the numerical solution becomes a direct consequence. As a further consequence, we observe that: as long as the numerical solution stays bounded at the previous time step, i.e., within $[-M, M]$ $(M>0)$, not necessarily $(-1,1)$, and its average stays between -1 and 1, there must exist a unique numerical solution which stays within $(-1,1)$ at the next time step. This leads to an interesting difference between the present results and those in [24], where the requirement for the initial data, namely, $\|\phi_0\|_\infty \le 1$, has to be imposed for the analysis to go through. On the other hand, the latter constraint is completely natural. Another new feature of the numerical analysis in this article is the theoretical justification of the energy stability. As a result of the unconditional energy stability, a uniform in time H_h^1 bound for the numerical solution could be derived. In addition, a detailed convergence analysis of the proposed numerical scheme could be derived, which gives an optimal rate error estimate in the $\ell^\infty(0,T;H_h^{-1})\cap\ell^2(0,T;H_h^1)$ norm. A key point in the analysis lies in the following subtle fact: since the nonlinear logarithmic term corresponds to a convex energy, the corresponding nonlinear error inner product is always non-negative. And also, the error estimate associated with the surface diffusion term indicates an $\ell^2(0,T;H_h^1)$ convergence. Because of the explicit treatment for the expansive term, this convergence estimate does not require the time step constraint, in comparison with the existing results [4,5,9,12,24].

On the other hand, all these positivity-preserving schemes are only first order accurate in time, which is not satisfactory in the practical computations. In turn, a higher order accurate in time, positivity-preserving numerical scheme is highly desired. In this article, we propose and analyze a second order accurate scheme for the CH model with Flory Huggins energy potential (1), with unique solvability, positivity-preserving property and energy stability established. In more details, we apply the implicit backward differentiation formula (BDF) concept to derive second order temporal accuracy, while the expansive term is treated by a second order explicit extrapolation formula. An additional term $A\Delta t\Delta_h(\phi^{k+1}-\phi^k)$ is added, which represents a second order Douglas-Dupont-type regularization, and a careful calculation shows that energy stability is guaranteed, provided the mild condition $A \ge \frac{1}{16}$ is enforced. Moreover, the singular nature of the logarithmic term enables us to theoretically derive the positivity-preserving property of this second order numerical scheme, which is the first such result in this area. And also, an H_h^{-1} inner product with the numerical error function leads to an optimal rate error estimate in the $\ell^\infty(0,T;H_h^{-1})\cap\ell^2(0,T;H_h^1)$ norm, with second order accuracy in both time and space.

The rest of the article is organized as follows. In Section 2 we propose the first order numerical scheme and state the corresponding theoretical results. The detailed proof for the positivity-preserving property of the numerical solution is provided in Section 3. Subsequently, the energy stability analysis is established in Section 4, and the optimal rate convergence analysis is presented in Section 5. The second order BDF scheme is outlined and analyzed in Section 6. Some numerical results are presented in Section 7, including a brief description of the 3-D multigrid solver. Finally, the concluding remarks are given in Section 8.

2. The first order numerical scheme

In the spatial discretization, the centered finite difference approximation is applied. We recall some of the basics of this methodology.

2.1. Discretization of space

We use the notation and results for some discrete functions and operators from [44,63,64]. Let $\Omega = (0, L_x) \times (0, L_y) \times (0, L_z)$, where for simplicity, we assume $L_x = L_y = L_z =: L > 0$. Let $N \in \mathbb{N}$ be given, and define the grid spacing $h := \frac{L}{N}$. We will assume – but only for simplicity of notation, ultimately – that the mesh spacing in the x, y, and z-directions are the same. We define the following two uniform, infinite grids with grid spacing $h > 0$:

$$E := \{p_{i+1/2} \mid i \in \mathbb{Z}\}, \quad C := \{p_i \mid i \in \mathbb{Z}\},$$

where $p_i = p(i) := (i - 1/2) \cdot h$. Consider the following 3-D discrete N^3-periodic function spaces:

$$\mathcal{C}_{\text{per}} := \left\{ v : C \times C \times C \to \mathbb{R} \;\middle|\; v_{i,j,k} = v_{i+\alpha N, j+\beta N, k+\gamma N},\ \forall i, j, k, \alpha, \beta, \gamma \in \mathbb{Z} \right\},$$
$$\mathcal{E}^{\text{x}}_{\text{per}} := \left\{ v : E \times C \times C \to \mathbb{R} \;\middle|\; v_{i+\frac{1}{2},j,k} = v_{i+\frac{1}{2}+\alpha N, j+\beta N, k+\gamma N},\ \forall i, j, k, \alpha, \beta, \gamma \in \mathbb{Z} \right\}.$$

Here we are using the identification $v_{i,j,k} = v(p_i, p_j, p_k)$, *et cetera*. The spaces $\mathcal{E}^{\text{y}}_{\text{per}}$ and $\mathcal{E}^{\text{z}}_{\text{per}}$ are analogously defined. The functions of $\mathcal{C}_{\text{per}}$ are called *cell centered functions*. The functions of $\mathcal{E}^{\text{x}}_{\text{per}}$, $\mathcal{E}^{\text{y}}_{\text{per}}$, and $\mathcal{E}^{\text{z}}_{\text{per}}$, are called *east-west*, *north-south*, and *up-down face-centered functions*, respectively. We also define the mean zero space

$$\mathring{\mathcal{C}}_{\text{per}} := \left\{ v \in \mathcal{C}_{\text{per}} \;\middle|\; 0 = \overline{v} := \frac{h^3}{|\Omega|} \sum_{i,j,k=1}^{m} v_{i,j,k} \right\}.$$

We define $\vec{\mathcal{E}}_{\text{per}} := \mathcal{E}^{\text{x}}_{\text{per}} \times \mathcal{E}^{\text{y}}_{\text{per}} \times \mathcal{E}^{\text{z}}_{\text{per}}$.

We now introduce the important difference and average operators on the spaces:

$$A_x v_{i+1/2,j,k} := \frac{1}{2}\left(v_{i+1,j,k} + v_{i,j,k}\right), \quad D_x v_{i+1/2,j,k} := \frac{1}{h}\left(v_{i+1,j,k} - v_{i,j,k}\right),$$
$$A_y v_{i,j+1/2,k} := \frac{1}{2}\left(v_{i,j+1,k} + v_{i,j,k}\right), \quad D_y v_{i,j+1/2,k} := \frac{1}{h}\left(v_{i,j+1,k} - v_{i,j,k}\right),$$
$$A_z v_{i,j,k+1/2} := \frac{1}{2}\left(v_{i,j,k+1} + v_{i,j,k}\right), \quad D_z v_{i,j,k+1/2} := \frac{1}{h}\left(v_{i,j,k+1} - v_{i,j,k}\right),$$

with $A_x,\ D_x : \mathcal{C}_{\text{per}} \to \mathcal{E}^{\text{x}}_{\text{per}}$, $A_y,\ D_y : \mathcal{C}_{\text{per}} \to \mathcal{E}^{\text{y}}_{\text{per}}$, $A_z,\ D_z : \mathcal{C}_{\text{per}} \to \mathcal{E}^{\text{z}}_{\text{per}}$. Likewise,

$$a_x v_{i,j,k} := \frac{1}{2}\left(v_{i+1/2,j,k} + v_{i-1/2,j,k}\right), \quad d_x v_{i,j,k} := \frac{1}{h}\left(v_{i+1/2,j,k} - v_{i-1/2,j,k}\right),$$
$$a_y v_{i,j,k} := \frac{1}{2}\left(v_{i,j+1/2,k} + v_{i,j-1/2,k}\right), \quad d_y v_{i,j,k} := \frac{1}{h}\left(v_{i,j+1/2,k} - v_{i,j-1/2,k}\right),$$
$$a_z v_{i,j,k} := \frac{1}{2}\left(v_{i,j,k+1/2} + v_{i,j,k-1/2}\right), \quad d_z v_{i,j,k} := \frac{1}{h}\left(v_{i,j,k+1/2} - v_{i,j,k-1/2}\right),$$

with $a_x,\ d_x : \mathcal{E}^{\text{x}}_{\text{per}} \to \mathcal{C}_{\text{per}}$, $a_y,\ d_y : \mathcal{E}^{\text{y}}_{\text{per}} \to \mathcal{C}_{\text{per}}$, and $a_z,\ d_z : \mathcal{E}^{\text{z}}_{\text{per}} \to \mathcal{C}_{\text{per}}$. The discrete gradient $\nabla_h : \mathcal{C}_{\text{per}} \to \vec{\mathcal{E}}_{\text{per}}$ is defined via

$$\nabla_h v_{i,j,k} = \left(D_x v_{i+1/2,j,k}, D_y v_{i,j+1/2,k}, D_z v_{i,j,k+1/2}\right),$$

and the discrete divergence $\nabla_h \cdot : \vec{\mathcal{E}}_{\text{per}} \to \mathcal{C}_{\text{per}}$ is defined via

$$\nabla_h \cdot \vec{f}_{i,j,k} = d_x f^x_{i,j,k} + d_y f^y_{i,j,k} + d_z f^z_{i,j,k},$$

where $\vec{f} = (f^x, f^y, f^z) \in \vec{\mathcal{E}}_{\text{per}}$. The standard 3-D discrete Laplacian, $\Delta_h : \mathcal{C}_{\text{per}} \to \mathcal{C}_{\text{per}}$, is given by

$$\begin{aligned}\Delta_h v_{i,j,k} :=& \nabla_h \cdot (\nabla_h \phi)_{i,j,k} = d_x(D_x v)_{i,j,k} + d_y(D_y v)_{i,j,k} + d_z(D_z v)_{i,j,k} \\ =& \frac{1}{h^2}\left(v_{i+1,j,k} + v_{i-1,j,k} + v_{i,j+1,k} + v_{i,j-1,k} + v_{i,j,k+1} + v_{i,j,k-1} - 6v_{i,j,k}\right).\end{aligned}$$

More generally, if $\mathcal{D}$ is a periodic *scalar* function that is defined at all of the face center points and $\vec{f} \in \vec{\mathcal{E}}_{\text{per}}$, then $\mathcal{D}\vec{f} \in \vec{\mathcal{E}}_{\text{per}}$, assuming point-wise multiplication, and we may define

$$\nabla_h \cdot \left(\mathcal{D}\vec{f}\right)_{i,j,k} = d_x\left(\mathcal{D}f^x\right)_{i,j,k} + d_y\left(\mathcal{D}f^y\right)_{i,j,k} + d_z\left(\mathcal{D}f^z\right)_{i,j,k}.$$

Specifically, if $v \in \mathcal{C}_{\text{per}}$, then $\nabla_h \cdot (\mathcal{D}\nabla_h\ \ ) : \mathcal{C}_{\text{per}} \to \mathcal{C}_{\text{per}}$ is defined point-wise via

$$\nabla_h \cdot \left(\mathcal{D}\nabla_h v\right)_{i,j,k} = d_x\left(\mathcal{D}D_x v\right)_{i,j,k} + d_y\left(\mathcal{D}D_y v\right)_{i,j,k} + d_z\left(\mathcal{D}D_z v\right)_{i,j,k}.$$

Now we are ready to define the following grid inner products:

$$\langle v, \xi\rangle_\Omega := h^3 \sum_{i,j,k=1}^{N} v_{i,j,k}\xi_{i,j,k}, \quad v,\ \xi \in \mathcal{C}_{\text{per}}, \quad [v,\xi]_{\text{x}} := \langle a_x(v\xi), 1\rangle_\Omega, \quad v,\ \xi \in \mathcal{E}^{\text{x}}_{\text{per}},$$
$$[v,\xi]_{\text{y}} := \langle a_y(v\xi), 1\rangle_\Omega, \quad v,\ \xi \in \mathcal{E}^{\text{y}}_{\text{per}}, \qquad [v,\xi]_{\text{z}} := \langle a_z(v\xi), 1\rangle_\Omega, \quad v,\ \xi \in \mathcal{E}^{\text{z}}_{\text{per}}.$$
$$\left[\vec{f}_1, \vec{f}_2\right]_\Omega := \left[f_1^x, f_2^x\right]_{\text{x}} + \left[f_1^y, f_2^y\right]_{\text{y}} + \left[f_1^z, f_2^z\right]_{\text{z}}, \quad \vec{f}_i = (f_i^x, f_i^y, f_i^z) \in \vec{\mathcal{E}}_{\text{per}},\ i = 1,2.$$

We define the following norms for cell-centered functions. If $v \in \mathcal{C}_{\text{per}}$, then $\|v\|_2^2 := \langle v, v\rangle_\Omega$; $\|v\|_p^p := \left\langle |v|^p, 1\right\rangle_\Omega$, for $1 \le p < \infty$, and $\|v\|_\infty := \max_{1\le i,j,k\le N}\left|v_{i,j,k}\right|$. We define norms of the gradient as follows: for $v \in \mathcal{C}_{\text{per}}$,

$$\|\nabla_h v\|_2^2 := [\nabla_h v, \nabla_h v]_\Omega = [D_x v, D_x v]_{\text{x}} + \left[D_y v, D_y v\right]_{\text{y}} + [D_z v, D_z v]_{\text{z}},$$

and, more generally, for $1 \le p < \infty$,

$$\|\nabla_h v\|_p := \left(\left[|D_x v|^p, 1\right]_{\text{x}} + \left[|D_y v|^p, 1\right]_{\text{y}} + \left[|D_z v|^p, 1\right]_{\text{z}}\right)^{\frac{1}{p}}. \tag{9}$$

Higher order norms can be defined. For example,

$$\|v\|_{H_h^1}^2 := \|v\|_2^2 + \|\nabla_h v\|_2^2, \quad \|v\|_{H_h^2}^2 := \|v\|_{H_h^1}^2 + \|\Delta_h v\|_2^2.$$

Lemma 2.1. *Let $\mathcal{D}$ be an arbitrary periodic, scalar function defined on all of the face center points. For any $\psi,\ v \in \mathcal{C}_{\text{per}}$ and any $\vec{f} \in \vec{\mathcal{E}}_{\text{per}}$, the following summation by parts formulas are valid:*

$$\left\langle \psi, \nabla_h \cdot \vec{f}\right\rangle_\Omega = -\left[\nabla_h\psi, \vec{f}\right]_\Omega, \quad \langle \psi, \nabla_h \cdot (\mathcal{D}\nabla_h v)\rangle_\Omega = -[\nabla_h\psi, \mathcal{D}\nabla_h v]_\Omega. \tag{10}$$

To facilitate the convergence analysis, we need to introduce a discrete analogue of the space $H_{per}^{-1}(\Omega)$, as outlined in [62]. Suppose that $\mathcal{D}$ is a positive, periodic scalar function defined at all of the face center points. For any $\phi \in \mathcal{C}_{\text{per}}$, there exists a unique $\psi \in \mathring{\mathcal{C}}_{\text{per}}$ that solves

$$\mathcal{L}_{\mathcal{D}}(\psi) := -\nabla_h \cdot (\mathcal{D}\nabla_h\psi) = \phi - \overline{\phi}, \tag{11}$$

where, recall, $\overline{\phi} := |\Omega|^{-1}\langle\phi, 1\rangle_\Omega$. We equip this space with a bilinear form: for any $\phi_1,\ \phi_2 \in \mathring{\mathcal{C}}_{\text{per}}$, define

$$\langle\phi_1, \phi_2\rangle_{\mathcal{L}_{\mathcal{D}}^{-1}} := [\mathcal{D}\nabla_h\psi_1, \nabla_h\psi_2]_\Omega, \tag{12}$$

where $\psi_i \in \mathring{\mathcal{C}}_{\text{per}}$ is the unique solution to

$$\mathcal{L}_{\mathcal{D}}(\psi_i) := -\nabla_h \cdot (\mathcal{D}\nabla_h\psi_i) = \phi_i, \quad i = 1,2. \tag{13}$$

The following identity [62] is easy to prove via summation-by-parts:

$$\langle\phi_1, \phi_2\rangle_{\mathcal{L}_{\mathcal{D}}^{-1}} = \left\langle\phi_1, \mathcal{L}_{\mathcal{D}}^{-1}(\phi_2)\right\rangle_\Omega = \left\langle\mathcal{L}_{\mathcal{D}}^{-1}(\phi_1), \phi_2\right\rangle_\Omega, \tag{14}$$

and since $\mathcal{L}_{\mathcal{D}}$ is symmetric positive definite, $\langle\ \cdot\ ,\ \cdot\ \rangle_{\mathcal{L}_{\mathcal{D}}^{-1}}$ is an inner product on $\mathring{\mathcal{C}}_{\text{per}}$ [62]. When $\mathcal{D} \equiv 1$, we drop the subscript and write $\mathcal{L}_1 = \mathcal{L}$, and in this case we usually write $\langle\ \cdot\ ,\ \cdot\ \rangle_{\mathcal{L}_{\mathcal{D}}^{-1}} =: \langle\ \cdot\ ,\ \cdot\ \rangle_{-1,h}$. In the general setting, the norm associated to this inner product is denoted $\|\phi\|_{\mathcal{L}_{\mathcal{D}}^{-1}} := \sqrt{\langle\phi,\phi\rangle_{\mathcal{L}_{\mathcal{D}}^{-1}}}$, for all $\phi \in \mathring{\mathcal{C}}_{\text{per}}$, but, if $\mathcal{D} \equiv 1$, we write $\|\cdot\|_{\mathcal{L}_{\mathcal{D}}^{-1}} =: \|\cdot\|_{-1,h}$.

2.2. The first order numerical scheme and the main theoretical results

We follow the idea of convexity splitting and consider the following semi-implicit, fully discrete schemes: given $\phi^n \in \mathcal{C}_{\rm per}$, find $\phi^{n+1}, \mu^{n+1} \in \mathcal{C}_{\rm per}$, such that

$$\frac{\phi^{n+1}-\phi^n}{\Delta t} = \nabla_h \cdot (\check{\mathcal{M}}^n \nabla_h \mu^{n+1}), \tag{15}$$

where

$$\mu^{n+1} = \ln(1+\phi^{n+1}) - \ln(1-\phi^{n+1}) - \theta_0 \phi^n - \varepsilon^2 \Delta_h \phi^{n+1}. \tag{16}$$

In more details, we require that $\check{\mathcal{M}}^n$ is defined at all of the face center points, which is accomplished via

$$\begin{aligned} &\check{\mathcal{M}}^n_{i+1/2,j,k} = \mathcal{M}(A_x \phi^n_{i+1/2,j,k}), \check{\mathcal{M}}^n_{i,j+1/2,k} = \mathcal{M}(A_y \phi^n_{i,j+1/2,k}), \\ &\check{\mathcal{M}}^n_{i,j,k+1/2} = \mathcal{M}(A_z \phi^n_{i,j,k+1/2}). \end{aligned} \tag{17}$$

Of course, a point-wise bound for the grid function ϕ^{n+1}, namely, $-1 < \phi^{n+1}_{i,j,k} < 1$, is needed so that the numerical scheme is well-defined. The main theoretical result is stated below, which guarantees that there exist unique numerical solutions for (15), so that the given bound is satisfied. In the first part, we assume that $\mathcal{M}(\phi) \equiv 1$; the non-constant mobility case will be analyzed in a later section.

Theorem 2.1. *Assume that $\mathcal{M}(\phi) \equiv 1$. Given $\phi^n \in \mathcal{C}_{\rm per}$, with $\|\phi^n\|_\infty \le M$, for some $M > 0$, and $|\overline{\phi^n}| < 1$, there exists a unique solution $\phi^{n+1} \in \mathcal{C}_{\rm per}$ to (15), with $\phi^{n+1} - \overline{\phi^n} \in \mathring{\mathcal{C}}_{\rm per}$ and $\|\phi^{n+1}\|_\infty < 1$.*

3. Theoretical justification of the positivity-preserving properties

3.1. Proof of Theorem 2.1

If solutions to the Cahn-Hilliard scheme (15) exist, it is clear that, for any $n \in \mathbb{N}$,

$$\overline{\phi}_0 := |\Omega|^{-1} \left\langle \phi^0, 1 \right\rangle_\Omega = |\Omega|^{-1} \langle \phi^1, 1 \rangle_\Omega = \cdots = |\Omega|^{-1} \langle \phi^n, 1 \rangle_\Omega = \overline{\phi}_n,$$

with $|\overline{\phi}_n| < 1$. Thus we expect $\langle \phi^n - \overline{\phi}_0, 1 \rangle_\Omega = 0$. For the proof of Theorem 2.1, we need the following technical lemma:

Lemma 3.1. *Suppose that $\phi_1, \phi_2 \in \mathcal{C}_{\rm per}$, with $\langle \phi_1 - \phi_2, 1 \rangle_\Omega = 0$, that is, $\phi_1 - \phi_2 \in \mathring{\mathcal{C}}_{\rm per}$, and assume that $\|\phi_1\|_\infty < 1$, $\|\phi_2\|_\infty \le M$. Then, we have the following estimate:*

$$\left\| \mathcal{L}^{-1}(\phi_1 - \phi_2) \right\|_\infty \le C_1, \tag{18}$$

where $C_1 > 0$ depends only upon M and Ω. In particular, C_1 is independent of the mesh spacing h.

Proof. Define $\psi := \phi_1 - \phi_2 \in \mathring{\mathcal{C}}_{\rm per}$. Thus $\|\psi\|_\infty < M + 1$. This fact implies that

$$\|\psi\|_2 = \|\phi_1 - \phi_2\|_2 \le (M+1)|\Omega|^{1/2}. \tag{19}$$

Meanwhile, we denote $v = \mathcal{L}^{-1}(\psi) \in \mathring{\mathcal{C}}_{\rm per}$, so that $\mathcal{L}(v) = \psi$ with $\overline{v} = 0$. Suppose that N is odd, for simplicity, and $N = 2K+1$. (The even case is handled in a very similar manner.) Since $v \in \mathcal{C}_{\rm per}$ it has the discrete Fourier representation of the form

$$v_{i,j,k} = \sum_{\ell,m,n=-K}^{K} \hat{v}^N_{\ell,m,n} \mathrm{e}^{2\pi i(\ell p_i + m p_j + n p_k)/L}, \tag{20}$$

where $p_i = (i - 1/2) \cdot h$ and $\hat{v}^N_{\ell,m,n}$ are the discrete Fourier coefficients given by the discrete Fourier transform (DFT):

$$\hat{v}^N_{i,j,k} := \frac{h^3}{L^3} \sum_{\ell,m,n=-K}^{K} v_{\ell,m,n} \mathrm{e}^{-2\pi i(\ell p_i + m p_j + n p_k)/L}.$$

Since $v \in \mathring{\mathcal{C}}_{\rm per}$, $\hat{v}^N_{0,0,0} = 0$. We define the Fourier interpolant of the grid function v as

$$\mathrm{v}(x,y,z) := \sum_{\ell,m,n=-K}^{K} \hat{v}^N_{\ell,m,n} \mathrm{e}^{2\pi i(\ell x+my+nz)/L}, \quad x,y,z \in \mathbb{R}, \tag{21}$$

and observe that $\mathrm{v} \in C^\infty_{\mathrm{per}}(\Omega)$. Parseval's identity (at both the discrete and continuous levels) implies that

$$\|v\|_2^2 = L^3 \sum_{\ell,m,n=-K}^{K} |\hat{v}^N_{\ell,m,n}|^2 = \|\mathrm{v}\|^2_{L^2(\Omega)}. \tag{22}$$

For the comparison between the discrete and continuous Laplacians, we start with the following Fourier expansions:

$$\begin{aligned} \Delta^x_h v_{i,j,k} &:= \frac{v_{i+1,j,k} - 2v_{i,j,k} + v_{i-1,j,k}}{h^2} \\ &= \sum_{\ell,m,n=-K}^{K} \mu_\ell \hat{v}^N_{\ell,m,n} \mathrm{e}^{2\pi i(\ell x_i + m y_j + n z_k)/L}, \end{aligned} \tag{23}$$

$$\partial^2_x \mathrm{v}(x,y,z) = \sum_{\ell,m,n=-K}^{K} \nu_\ell \hat{v}^N_{\ell,m,n} \mathrm{e}^{2\pi i(\ell x+my+nz)/L}, \tag{24}$$

with

$$\mu_\ell = -\frac{4\sin^2 \frac{\ell\pi h}{L}}{h^2}, \quad \nu_\ell = -\frac{4\ell^2\pi^2}{L^2}. \tag{25}$$

In turn, an application of Parseval's identity yields

$$\left\| \Delta^x_h v \right\|_2^2 = L^3 \sum_{\ell,m,n=-K}^{K} |\mu_\ell|^2 |\hat{v}^N_{\ell,m,n}|^2, \tag{26}$$

$$\left\| \partial^2_x \mathrm{v} \right\|_{L^2}^2 = L^3 \sum_{\ell,m,n=-K}^{K} |\nu_\ell|^2 |\hat{v}^N_{\ell,m,n}|^2. \tag{27}$$

The comparison of Fourier eigenvalues shows that

$$\frac{4}{\pi^2}|\nu_\ell| \le |\mu_\ell| \le |\nu_\ell|, \quad \text{for} \quad -K \le \ell \le K. \tag{28}$$

This indicates that

$$\frac{4}{\pi^2} \left\| \partial^2_x \mathrm{v} \right\|_{L^2} \le \left\| \Delta^x_h v \right\|_2 \le \left\| \partial^2_x \mathrm{v} \right\|_{L^2}. \tag{29}$$

Similar estimates can be derived to reveal that

$$\frac{4}{\pi^2}\|\Delta \mathrm{v}\|_{L^2} \le \|\Delta_h v\|_2 = \|\psi\|_2 \le \|\Delta \mathrm{v}\|_{L^2}, \tag{30}$$

which in turn yields that $\|\Delta \mathrm{v}\|_{L^2} \le \frac{(M+1)\pi^2|\Omega|^{1/2}}{4}$.

Meanwhile, the following identity is obvious:

$$\int_\Omega \mathrm{v}\, d\mathbf{x} = 0, \quad \text{since} \quad \hat{v}^N_{0,0,0} = 0. \tag{31}$$

Subsequently, an application of elliptic regularity implies that

$$\|\mathrm{v}\|_{H^2} \le C \left(\left| \int_\Omega \mathrm{v}\, d\mathbf{x} \right| + \|\Delta \mathrm{v}\|_{L^2} \right) \le C_0 (M+1)|\Omega|^{1/2}, \tag{32}$$

for some constant $C_0 > 0$ that only depends upon Ω. Since the grid function v is the projection of the smooth function v into the cell-centered grid, the following discrete ℓ^∞ bound is clear:

$$\|v\|_\infty \le \|\mathrm{v}\|_{L^\infty} \le C\|\mathrm{v}\|_{H^2} \le C_0(M+1)|\Omega|^{1/2}, \tag{33}$$

in which the 3-D Sobolev embedding has been used in the second step. The proof of Lemma 3.1 is completed by taking $C_1 := C_0(M+1)|\Omega|^{1/2}$. □

Now we proceed into the proof of Theorem 2.1.

Proof. The numerical solution of (15) is a minimizer of the following discrete energy functional:

$$\mathcal{J}^n(\phi) := \frac{1}{2\Delta t}\left\|\phi-\phi^n\right\|_{-1,h}^2 + \langle 1+\phi, \ln(1+\phi)\rangle_\Omega + \langle 1-\phi, \ln(1-\phi)\rangle_\Omega + \frac{\varepsilon^2}{2}\|\nabla_h\phi\|_2^2 - \theta_0\langle\phi,\phi^n\rangle_\Omega, \tag{34}$$

over the admissible set

$$A_h := \left\{\phi\in\mathcal{C}_{\text{per}} \;\middle|\; \|\phi\|_\infty\le 1, \quad \langle\phi-\overline{\phi}_0, 1\rangle_\Omega = 0\right\}\subset\mathbb{R}^{N^3}.$$

Observe that $\mathcal{J}^n$ is a strictly convex function over this domain.

To facilitate the analysis below, we transform the minimization problem into an equivalent one. Consider the functional

$$\mathcal{F}^n(\varphi) := \mathcal{J}^n(\varphi+\overline{\phi}_0) \tag{35}$$

$$= \frac{1}{2\Delta t}\left\|\varphi+\overline{\phi}_0-\phi^n\right\|_{-1,h}^2 + \left\langle 1+\varphi+\overline{\phi}_0, \ln(1+\varphi+\overline{\phi}_0)\right\rangle_\Omega + \left\langle 1-\varphi-\overline{\phi}_0, \ln(1-\varphi-\overline{\phi}_0)\right\rangle_\Omega + \frac{\varepsilon^2}{2}\|\nabla_h\varphi\|_2^2 - \theta_0\left\langle\varphi+\overline{\phi}_0,\phi^n\right\rangle_\Omega, \tag{36}$$

defined on the set

$$\mathring{A}_h := \left\{\varphi\in\mathring{\mathcal{C}}_{\text{per}} \;\middle|\; -1+\overline{\phi}_0\le\varphi\le 1-\overline{\phi}_0\right\}\subset\mathbb{R}^{N^3}.$$

If $\varphi\in\mathring{A}_h$ minimizes $\mathcal{F}^n$, then $\phi := \varphi+\overline{\phi}_0\in A_h$ minimizes $\mathcal{J}^n$, and *vice versa*. Next, we prove that there exists a minimizer of $\mathcal{F}^n$ over the domain $\mathring{A}_h$. Similar to our previous arguments, we consider the following closed domain: for $\delta\in(0, 1/2)$,

$$\mathring{A}_{h,\delta} := \left\{\varphi\in\mathring{\mathcal{C}}_{\text{per}} \;\middle|\; \delta-1-\overline{\phi}_0\le\varphi\le 1-\delta-\overline{\phi}_0\right\}\subset\mathbb{R}^{N^3}. \tag{37}$$

Since $\mathring{A}_{h,\delta}$ is a bounded, compact, and convex set in the subspace $\mathring{\mathcal{C}}_{\text{per}}$, there exists a (not necessarily unique) minimizer of $\mathcal{F}^n$ over $\mathring{A}_{h,\delta}$. The key point of the positivity analysis is that such a minimizer could not occur on the boundary of $\mathring{A}_{h,\delta}$, if δ is sufficiently small. To be more explicit, by the boundary of $\mathring{A}_{h,\delta}$, we mean the locus of points $\psi\in\mathring{A}_{h,\delta}$ such that $\left\|\psi+\overline{\phi}_0\right\|_\infty = 1-\delta$, precisely.

To get a contradiction, suppose that the minimizer of $\mathcal{F}^n$, call it $\varphi^\star$ occurs at a boundary point of $\mathring{A}_{h,\delta}$. There is at least one grid point $\vec{\alpha}_0 = (i_0, j_0, k_0)$ such that $|\varphi^\star_{\vec{\alpha}_0}+\overline{\phi}_0| = 1-\delta$. First, let us assume, that $\varphi^\star_{\vec{\alpha}_0}+\overline{\phi}_0 = \delta-1$, so that the grid function $\varphi^\star$ has a global minimum at $\vec{\alpha}_0$. Suppose that $\vec{\alpha}_1 = (i_1, j_1, k_1)$ is a grid point at which $\varphi^\star$ achieves its maximum. By the fact that $\overline{\varphi^\star} = 0$, it is obvious that

$$1-\delta\ge\varphi^\star_{\vec{\alpha}_1}+\overline{\phi}_0\ge\overline{\phi}_0.$$

Since $\mathcal{F}^n$ is smooth over $\mathring{A}_{h,\delta}$, for all $\psi\in\mathring{\mathcal{C}}_{\text{per}}$, the directional derivative is

$$d_s\mathcal{F}^n(\varphi^\star+s\psi)|_{s=0} = \left\langle\ln(1+\varphi^\star+\overline{\phi}_0)-\ln(1-\varphi^\star-\overline{\phi}_0),\psi\right\rangle_\Omega - \left\langle\theta_0\phi^n+\varepsilon^2\Delta_h\varphi^\star,\psi\right\rangle_\Omega + \frac{1}{\Delta t}\left\langle(-\Delta_h)^{-1}\left(\varphi^\star-\phi^n+\overline{\phi}_0\right),\psi\right\rangle_\Omega.$$

This time, let us pick the direction $\psi\in\mathring{\mathcal{C}}_{\text{per}}$, such that

$$\psi_{i,j,k} = \delta_{i,i_0}\delta_{j,j_0}\delta_{k,k_0} - \delta_{i,i_1}\delta_{j,j_1}\delta_{k,k_1}.$$

Then the derivative may be expressed as

$$\begin{aligned}\frac{1}{h^3}d_s\mathcal{F}^n(\varphi^\star+s\psi)|_{s=0} = {}& \ln(1+\varphi^\star_{\vec{\alpha}_0}+\overline{\phi}_0)-\ln(1-\varphi^\star_{\vec{\alpha}_0}-\overline{\phi}_0)-\ln(1+\varphi^\star_{\vec{\alpha}_1}+\overline{\phi}_0)+\ln(1-\varphi^\star_{\vec{\alpha}_1}-\overline{\phi}_0)\\ &-\theta_0(\phi^n_{\vec{\alpha}_0}-\phi^n_{\vec{\alpha}_1})-\varepsilon^2(\Delta_h\varphi^\star_{\vec{\alpha}_0}-\Delta_h\varphi^\star_{\vec{\alpha}_1})+\frac{1}{\Delta t}(-\Delta_h)^{-1}(\varphi^\star-\phi^n+\overline{\phi}_0)_{\vec{\alpha}_0}\\ &-\frac{1}{\Delta t}(-\Delta_h)^{-1}(\varphi^\star-\phi^n+\overline{\phi}_0)_{\vec{\alpha}_1}.\end{aligned} \tag{38}$$

For simplicity, now let us write $\phi^\star := \varphi^\star+\overline{\phi}_0$. Since $\phi^\star_{\vec{\alpha}_0} = -1+\delta$ and $\phi^\star_{\vec{\alpha}_1}\ge\overline{\phi}_0$, we have

$$\ln(1+\phi^\star_{\vec{\alpha}_0})-\ln(1-\phi^\star_{\vec{\alpha}_0})-\ln(1+\phi^\star_{\vec{\alpha}_1})+\ln(1-\phi^\star_{\vec{\alpha}_1})\le\ln\frac{\delta}{2-\delta}-\ln\frac{1+\overline{\phi}_0}{1-\overline{\phi}_0}. \tag{39}$$

Since $\phi^\star$ takes a minimum at the grid point $\vec{\alpha}_0$, with $\phi^\star_{\vec{\alpha}_0} = -1 + \delta \le \phi^\star_{i,j,k}$, for any (i, j, k), and a maximum at the grid point $\vec{\alpha}_1$, with $\phi^\star_{\vec{\alpha}_1} \ge \phi^\star_{i,j,k}$, for any (i, j, k),

$$\Delta_h \phi^\star_{\vec{\alpha}_0} \ge 0, \quad \Delta_h \phi^\star_{\vec{\alpha}_1} \le 0. \tag{40}$$

For the numerical solution ϕ^n at the previous time step, the *a priori* assumption $\left\| \phi^n \right\|_\infty \le M$ indicates that

$$-2M \le \phi^n_{\vec{\alpha}_0} - \phi^n_{\vec{\alpha}_1} \le 2M. \tag{41}$$

For the last two terms appearing in (38), we apply Lemma 3.1 and obtain

$$-2C_1 \le (-\Delta_h)^{-1}(\phi^\star - \phi^n)_{\vec{\alpha}_0} - (-\Delta_h)^{-1}(\phi^\star - \phi^n)_{\vec{\alpha}_1} \le 2C_1. \tag{42}$$

Consequently, a substitution of (39) – (42) into (38) yields the following bound on the directional derivative:

$$\frac{1}{h^3} d_s \mathcal{F}^n(\varphi^\star + s\psi)|_{s=0} \le \ln \frac{\delta}{2-\delta} - \ln \frac{1+\overline{\phi}_0}{1-\overline{\phi}_0} + 2M\theta_0 + 2C_1 \Delta t^{-1}. \tag{43}$$

We denote $C_2 = 2M\theta_0 + 2C_1 \Delta t^{-1}$. Note that C_2 is a constant for a fixed Δt, though it becomes singular as $\Delta t \to 0$. However, for any fixed Δt, we may choose $\delta \in (0, 1/2)$ sufficiently small so that

$$\ln \frac{\delta}{2-\delta} - \ln \frac{1+\overline{\phi}_0}{1-\overline{\phi}_0} + C_2 < 0. \tag{44}$$

This in turn shows that, provided δ satisfies (44),

$$\frac{1}{h^3} d_s \mathcal{F}^n(\varphi^\star + s\psi)|_{s=0} < 0. \tag{45}$$

As before, this contradicts the assumption that $\mathcal{F}^n$ has a minimum at $\varphi^\star$, since the directional derivative is negative in a direction pointing into the interior of $\mathring{A}_{h,\delta}$.

Using very similar arguments, we can also prove that the global minimum of $\mathcal{F}^n$ over $\mathring{A}_{h,\delta}$ could not occur at a boundary point $\varphi^\star$ such that $\varphi^\star_{\vec{\alpha}_0} + \overline{\phi}_0 = 1 - \delta$, for some $\vec{\alpha}_0$, so that the grid function $\varphi^\star$ has a global maximum at $\vec{\alpha}_0$. The details are left to interested readers.

A combination of these two facts shows that, the global minimum of $\mathcal{F}^n$ over $\mathring{A}_{h,\delta}$ could only possibly occur at interior point $\varphi \in (\mathring{A}_{h,\delta})^o \subset (\mathring{A}_h)^o$. We conclude that there must be a solution $\phi = \varphi + \overline{\phi}_0 \in A_h$ that minimizes $\mathcal{J}^n$ over A_h, which is equivalent to the numerical solution of (15), (16). The existence of the numerical solution is established.

In addition, since $\mathcal{J}^n$ is a strictly convex function over A_h, the uniqueness analysis for this numerical solution is straightforward. The proof of Theorem 2.1 is complete. □

Remark 3.1. The positivity-preserving analysis is based on a key fact that the singular nature of the logarithmic term around the values of -1 and 1 prevents the numerical solution reaching these singular values. As a result, the point-wise positivity for the logarithmic arguments could be derived as long as the numerical solution at the previous time step stays bounded between $-M$ and M (even if $M > 1$), and the initial average stays between -1 and 1. This is a modest improvement to the results in [24], in which the authors constructed a cut-off energy functional to avoid the singularity.

Remark 3.2. For the 3-D Allen-Cahn flow (2), a uniform separation bound could be derived, following a maximum principle type argument. However, for the Cahn-Hilliard flow, such a uniform bound is not available for the corresponding numerical solution (15), (16) any more, since the maximum principle could not be directly applied to an H^{-1} gradient flow. In addition, the mass conservation constraint has made the corresponding analysis more involved.

Remark 3.3. For the Cahn-Hilliard flow, lack of maximum principle has been an essential mathematical challenge. To overcome this difficulty, we have to obtain the point-wise bound for the linear chemical potential part. With the help of the *a priori* ℓ^∞ bound of the numerical solution we are investigating, an $O(\Delta t^{-1})$ estimate is derived for such a bound, which is contained in the form of C_2. Such a bound is a fixed constant for a fixed Δt, while it becomes singular as $\Delta t \to 0$.

Another key idea of this analysis should also be mentioned: although the nonlinear term contains a singular limit as ϕ approaches either -1 or 1, the convexity of this nonlinear potential has greatly aided in the positivity analysis.

Remark 3.4. In addition to the positivity-preserving property, the semi-implicit nature of our proposed scheme: implicit treatment for the logarithmic terms and the surface diffusion term, combined with an explicit treatment for the linear stretching/expansive term, ensures the unique solvability. In comparison, for the fully implicit scheme analyzed in [24], the unique solvability is only available under a time step constraint: $\Delta t \le \frac{4\varepsilon^2}{\theta_0^2}$. In fact, the existence of the positivity-preserving numerical solution could also be established for the fully implicit Euler scheme, using the same idea presented in this section. Only the uniqueness analysis of the numerical solution requires such a time step constraint.

Remark 3.5. For simplicity of presentation, we only analyze the finite difference scheme over a rectangular domain in this article. The idea of this positivity analysis could be similarly extended to the finite element and pseudo-spectral spatial approximations, as well as the case of a general domain. Some technical difficulties, such as the projection of the nonlinear term (instead of the point-wise value in finite difference method), are expected to be overcome in an appropriate manner. The details may be considered in the future works.

3.2. The positivity preserving property in the non-constant mobility case

In this subsection we look at the numerical scheme (15), (16) with a nonconstant mobility, but with the strict positivity assumption that $\mathcal{M}(x) \geq \mathcal{M}_0 > 0$, for all $x \in [-1, 1]$. The positivity-preserving property of this numerical scheme is stated below. The details of the proof are provided in Appendix B.

Theorem 3.1. *Assume that $\mathcal{M}(x) \geq \mathcal{M}_0 > 0$, for all $x \in [-1, 1]$. Given $\phi^n \in \mathcal{C}_{\text{per}}$, with $\left\| \phi^n \right\| \leq M$, for some $M > 0$, and $\left| \overline{\phi^n} \right| < 1$, there exists a unique solution $\phi^{n+1} \in \mathcal{C}_{\text{per}}$ to (15), with $\phi^{n+1} - \overline{\phi^n} \in \mathring{\mathcal{C}}_{\text{per}}$ and $\left\| \phi^{n+1} \right\|_\infty < 1$.*

4. Unconditional energy stability and uniform in time H_h^1 bound

The discrete energy is defined as

$$E_h(\phi) = \langle 1+\phi, \ln(1+\phi) \rangle_\Omega + \langle 1-\phi, \ln(1-\phi) \rangle_\Omega + \frac{\varepsilon^2}{2} \| \nabla_h \phi \|_2^2 - \frac{\theta_0}{2} \| \phi \|_2^2. \tag{46}$$

For the numerical scheme for the Cahn-Hilliard equation (15), (16), the existence and unique solvability (so that the numerical solution stays within $(-1, 1)$ at a point-wise level) have been established in Theorem 3.1. Because the scheme uses a convex-concave decomposition, it is unconditionally energy stability. This result is stated in the following theorem.

Theorem 4.1. *For simplicity, suppose that $N = 2K + 1$, and let $\mathcal{P}_N : C_{\text{per}}(\Omega) \to \mathcal{B}_K(\Omega)$ denote the Fourier projection operator, where $\mathcal{B}_K$ is space of Ω-periodic (complex) trigonometric polynomials of degree up to and including K. By $\mathcal{P}_h : C_{\text{per}}(\Omega) \to \mathcal{C}_{\text{per}}$ denote the canonical grid projection operator. Suppose that $\phi^0 := \mathcal{P}_h(\mathcal{P}_N \Phi)$, where $\Phi \in C^6_{\text{per}}(\Omega)$ and $\| \Phi \|_{L^\infty} < 1$. Then $(\Phi, 1)_{L^2} = \langle \phi^0, 1 \rangle_\Omega$, and, for any $\Delta t > 0$, $h > 0$, and $m \in \mathbb{N}$,*

$$E_h(\phi^m) + \left[\check{\mathcal{M}}^{m-1} \nabla_h \mu^m, \nabla_h \mu^m \right]_\Omega \leq E_h(\phi^{m-1}), \tag{47}$$

so that $E_h(\phi^m) \leq E_h(\phi^0) \leq C_6$, with $C_6 > 0$ independent of h. Therefore, since $-\frac{\theta_0}{2}|\Omega| + \frac{\varepsilon^2}{2} \| \nabla_h \phi^m \|_2^2 \leq E_h(\phi^m)$, we have

$$\left\| \nabla_h \phi^m \right\|_2 \leq \sqrt{2C_6 + \theta_0 |\Omega|} \varepsilon^{-1} =: C_7, \quad \forall m \in \mathbb{N}. \tag{48}$$

Proof. Taking an inner product with (15) by μ^{n+1} yields

$$\langle \phi^{n+1} - \phi^n, \mu^{n+1} \rangle_\Omega + \left[\check{\mathcal{M}}^n \nabla_h \mu^{n+1}, \nabla_h \mu^{n+1} \right]_\Omega = 0. \tag{49}$$

On the other hand, the convexity of the energy terms $\langle 1+\phi, \ln(1+\phi) \rangle$, $\langle 1-\phi, \ln(1-\phi) \rangle$ and $\| \nabla_h \phi \|_2^2$, as well as the concave property of $-\| \phi \|_2^2$, imply that

$$\begin{aligned} &\langle \phi^{n+1} - \phi^n, \ln(1+\phi^{n+1}) - \ln(1-\phi^{n+1}) \rangle_\Omega \\ &\geq \langle 1+\phi^{n+1}, \ln(1+\phi^{n+1}) \rangle + \langle 1-\phi^{n+1}, \ln(1-\phi^{n+1}) \rangle_\Omega \\ &\quad - \langle 1+\phi^n, \ln(1+\phi^n) \rangle_\Omega - \langle 1-\phi^n, \ln(1-\phi^n) \rangle_\Omega, \end{aligned} \tag{50}$$

$$\langle \phi^{n+1} - \phi^n, -\Delta_h \phi^{n+1} \rangle_\Omega \geq \frac{1}{2} (\| \nabla_h \phi^{n+1} \|_2^2 - \| \nabla_h \phi^n \|_2^2), \tag{51}$$

$$\langle \phi^{n+1} - \phi^n, -\phi^n \rangle_\Omega \geq -\frac{1}{2} (\| \phi^{n+1} \|_2^2 - \| \phi^n \|_2^2). \tag{52}$$

In turn, a substitution of (50)-(52) into (49) leads to (47) (with $m = n + 1$), so that the unconditional energy stability is proved.

In addition, the discrete H^1 estimate (48) comes from a direct energy inequality, $-\frac{\theta_0}{2}|\Omega| + \frac{\varepsilon^2}{2} \| \nabla_h \phi^m \|_2^2 \leq E_h(\phi^m)$, for any $m \geq 0$. This completes the proof of Theorem 4.1. □

Remark 4.1. The unconditional energy stability of the proposed scheme (15), (16) follows from the convex-concave decomposition of the energy, an idea popularized in Eyre's work [34]. The method has been applied to the phase field crystal (PFC) equation and the modified version [62,64]; epitaxial thin film growth models [17,61]; non-local gradient model [42]; the Cahn-Hilliard model coupled with fluid flow [18,27,36,53,63]; *et cetera*. Second order accurate energy stable schemes have also been reported in recent years, based on either a secant/Crank-Nicolson or BDF approach. See, for example, [10,11,19–21,29,28,44–46,59,41,66]. In particular, for the multi-component Cahn-Hilliard model, the related works could also be found in [6,7].

Remark 4.2. For the CH model with Flory Huggins energy potential, there have been some works to address the energy stability in the existing literature [47,51,52,57,67]. However, the positivity-preserving property has not been theoretically justified for these numerical works, so that the existence of the numerical solutions in these works is not available at a theoretical level.

5. Optimal rate convergence analysis in $\ell^\infty(0,T;H^{-1})\cap\ell^2(0,T;H^1)$

For simplicity of presentation, we assume $\mathcal{M}\equiv 1$ in this section; the convergence analysis for the non-constant mobility case will be considered in future works.

Let Φ be the exact solution for the Cahn-Hilliard flow (3) – (4). With initial data with sufficient regularity, we could assume that the exact solution has regularity of class $\mathcal{R}$:

$$\Phi\in\mathcal{R}:=H^2\left(0,T;C_{\text{per}}(\Omega)\right)\cap H^1\left(0,T;C^2_{\text{per}}(\Omega)\right)\cap L^\infty\left(0,T;C^6_{\text{per}}(\Omega)\right). \tag{53}$$

Define $\Phi_N(\cdot,t):=\mathcal{P}_N\Phi(\cdot,t)$, the (spatial) Fourier projection of the exact solution into $\mathcal{B}^K$, the space of trigonometric polynomials of degree to and including K. The following projection approximation is standard: if $\Phi\in L^\infty(0,T;H^\ell_{\text{per}}(\Omega))$,

$$\|\Phi_N-\Phi\|_{L^\infty(0,T;H^k)}\le Ch^{\ell-k}\|\Phi\|_{L^\infty(0,T;H^\ell)},\quad \forall\, 0\le k\le\ell. \tag{54}$$

By Φ_N^m, Φ^m we denote $\Phi_N(\cdot,t_m)$ and $\Phi(\cdot,t_m)$, respectively, with $T_m=m\cdot\Delta t$. Since $\Phi_N\in\mathcal{B}^K$, the mass conservative property is available at the discrete level:

$$\overline{\Phi_N^m}=\frac{1}{|\Omega|}\int_\Omega\Phi_N(\cdot,t_m)\,d\mathbf{x}=\frac{1}{|\Omega|}\int_\Omega\Phi_N(\cdot,t_{m-1})\,d\mathbf{x}=\overline{\Phi_N^{m-1}},\quad\forall\, m\in\mathbb{N}. \tag{55}$$

On the other hand, the solution of (15), (16) is also mass conservative at the discrete level:

$$\overline{\phi^m}=\overline{\phi^{m-1}},\quad\forall\, m\in\mathbb{N}. \tag{56}$$

As indicated before, we use the mass conservative projection for the initial data: $\phi^0=\mathcal{P}_h\Phi_N(\cdot,t=0)$, that is

$$\phi^0_{i,j,k}:=\Phi_N(p_i,p_j,p_k,t=0), \tag{57}$$

The error grid function is defined as

$$\tilde\phi^m:=\mathcal{P}_h\Phi_N^m-\phi^m,\quad\forall\, m\in\{0,1,2,3,\cdots\}. \tag{58}$$

Therefore, it follows that $\overline{\tilde\phi^m}=0$, for any $m\in\{0,1,2,3,\cdots\}$, so that the discrete norm $\|\cdot\|_{-1,h}$ is well defined for the error grid function.

Theorem 5.1. *Given initial data $\Phi(\cdot,t=0)\in C^6_{\text{per}}(\Omega)$, suppose the exact solution for Cahn-Hilliard equation (3)-(4) is of regularity class $\mathcal{R}$. Then, provided Δt and h are sufficiently small, for all positive integers n, such that $t_n\le T$, we have*

$$\|\tilde\phi^n\|_{-1,h}+\left(\varepsilon^2\Delta t\sum_{m=1}^n\|\nabla_h\tilde\phi^m\|_2^2\right)^{1/2}\le C(\Delta t+h^2), \tag{59}$$

where $C>0$ is independent of n, Δt, and h.

Proof. A careful consistency analysis indicates the following truncation error estimate:

$$\frac{\Phi_N^{n+1}-\Phi_N^n}{\Delta t}=\Delta_h\left(\ln(1+\Phi_N^{n+1})-\ln(1-\Phi_N^{n+1})-\theta_0\Phi_N^n-\varepsilon^2\Delta_h\Phi_N^{n+1}\right)+\tau^n, \tag{60}$$

with $\|\tau^n\|_{-1,h}\le C(\Delta t+h^2)$. Observe that in equation (60), and from this point forward, we drop the operator $\mathcal{P}_h$, which should appear in front of Φ_N, for simplicity.

Subtracting the numerical scheme (15) from (60) gives

$$\frac{\tilde{\phi}^{n+1}-\tilde{\phi}^{n}}{\Delta t}=\Delta_h\Big((\ln(1+\Phi_N^{n+1})-\ln(1+\phi^{n+1}))-(\ln(1-\Phi_N^{n+1})-\ln(1-\phi^{n+1}))-\theta_0\tilde{\phi}^{n}-\varepsilon^2\Delta_h\tilde{\phi}^{n+1}\Big)+\tau^n. \tag{61}$$

Since the numerical error function has zero-mean, we see that $(-\Delta_h)^{-1}\tilde{\phi}^m$ is well-defined, for any $k\geq 0$. Taking a discrete inner product with (61) by $2(-\Delta_h)^{-1}\tilde{\phi}^{n+1}$ yields

$$\begin{aligned}&\|\tilde{\phi}^{n+1}\|_{-1,h}^2-\|\tilde{\phi}^{n}\|_{-1,h}^2+\|\tilde{\phi}^{n+1}-\tilde{\phi}^{n}\|_{-1,h}^2-2\varepsilon^2\Delta t\left\langle\tilde{\phi}^{n+1},\Delta_h\tilde{\phi}^{n+1}\right\rangle_\Omega\\&\quad+2\Delta t\left\langle\ln(1+\Phi_N^{n+1})-\ln(1+\phi^{n+1}),\tilde{\phi}^{n+1}\right\rangle_\Omega\\&\quad-2\Delta t\left\langle\ln(1-\Phi_N^{n+1})-\ln(1-\phi^{n+1}),\tilde{\phi}^{n+1}\right\rangle_\Omega\\&\qquad=2\theta_0\Delta t\left\langle\tilde{\phi}^{n},\tilde{\phi}^{n+1}\right\rangle_\Omega+2\Delta t\langle\tau^n,\tilde{\phi}^{n+1}\rangle_{-1,h}.\end{aligned} \tag{62}$$

The estimate for the term associated with the surface diffusion is straightforward:

$$-\langle\tilde{\phi}^{n+1},\Delta_h\tilde{\phi}^{n+1}\rangle_\Omega=\|\nabla_h\tilde{\phi}^{n+1}\|_2^2. \tag{63}$$

For the nonlinear inner product, the fact that $-1<\phi^{n+1}<1$, $-1<\Phi^{n+1}<1$ (at a point-wise level) yields the following result:

$$\left\langle\ln(1+\Phi_N^{n+1})-\ln(1+\phi^{n+1}),\tilde{\phi}^{n+1}\right\rangle_\Omega\geq 0, \tag{64}$$

$$-\left\langle\ln(1-\Phi_N^{n+1})-\ln(1-\phi^{n+1}),\tilde{\phi}^{n+1}\right\rangle_\Omega\geq 0, \tag{65}$$

due to the fact that ln is an increasing function. In other words, the convexity of the nonlinear term plays an essential role in this analysis. For the inner product associated with the concave part, the following estimate is derived:

$$2\theta_0\left\langle\tilde{\phi}^{n},\tilde{\phi}^{n+1}\right\rangle_\Omega\leq 2\theta_0\|\tilde{\phi}^{n}\|_{-1,h}\|\nabla_h\tilde{\phi}^{n+1}\|_2\leq\theta_0^2\varepsilon^{-2}\|\tilde{\phi}^{n}\|_{-1,h}^2+\varepsilon^2\|\nabla_h\tilde{\phi}^{n+1}\|_2^2. \tag{66}$$

The term associated with the truncation error can be controlled in a standard way:

$$2\langle\tau^n,\tilde{\phi}^{n+1}\rangle_{-1,h}\leq 2\|\tau^n\|_{-1,h}\cdot\|\tilde{\phi}^{n+1}\|_{-1,h}\leq\|\tau^n\|_{-1,h}^2+\|\tilde{\phi}^{n+1}\|_{-1,h}^2. \tag{67}$$

Using estimates (63) – (67) in (62) yields

$$\|\tilde{\phi}^{n+1}\|_{-1,h}^2-\|\tilde{\phi}^{n}\|_{-1,h}^2+\varepsilon^2\Delta t\|\nabla_h\tilde{\phi}^{n+1}\|_2^2\leq\theta_0^2\varepsilon^{-2}\Delta t\|\tilde{\phi}^{n}\|_{-1,h}^2+\Delta t\|\tilde{\phi}^{n+1}\|_{-1,h}^2+\Delta t\|\tau^n\|_{-1,h}^2. \tag{68}$$

Finally, an application of a discrete Gronwall inequality results in the desired convergence estimate:

$$\|\tilde{\phi}^{n+1}\|_{-1,h}+\left(\varepsilon^2\Delta t\sum_{k=0}^{n+1}\|\nabla_h\tilde{\phi}^{m}\|_2^2\right)^{1/2}\leq C(\Delta t+h^2), \tag{69}$$

where $C>0$ is independent of Δt, h, and n. This completes the proof of the theorem. □

Remark 5.1. For the Cahn-Hilliard equation with logarithmic potential, there have been some existing works of error estimate [4,5,9] in the framework of finite element analysis, with implicit Euler method in the temporal discretization. Again, the time step constraint $\Delta t\leq\frac{4\varepsilon^2}{\theta_0^2}$ has to be imposed to ensure the positivity-preserving property of the numerical scheme, while no constraint is needed in the convergence analysis of our proposed scheme.

Remark 5.2. In the truncation error estimate (60), a detailed Taylor expansion reveals that, $\|\tau^n\|_{-1,h}$ is associated with the H_h^{-1} norm $\partial_{tt}\Phi_N$, a discrete $\|\cdot\|_2$ norm of $\partial_t\nabla_h\Phi_N$, the $L^\infty(0,T;H^5)$ norm of Φ_N, as well as the projection errors. In particular, its dependence on the higher order temporal and spatial derivatives of the exact solution Φ has played an important role in the optimal rate convergence analysis. Moreover, a bound of the higher order derivatives of the exact solution for the Cahn-Hilliard flow relies on the phase separation, i.e., a uniform distance between Φ and the singular limit values (-1 and 1) is available for the exact solution, so that a singularity in the higher order derivatives is avoided.

In fact, the regularity assumption (53) has indicated such a phase separation in order to keep the higher order derivatives bounded. For 1-D and 2-D Cahn-Hilliard flows, the phase separation has been justified at a theoretical level [38,22,54], so that the truncation error estimate could go through. For the 3-D equation, although the phase separation is not available globally in time, one can always assume a local-in-time property, if a separation profile is taken for the initial data, so that the presented convergence analysis could also be derived in a local-in-time manner, before the higher order derivatives become singular.

6. The second order numerical scheme

We propose the following second order scheme for the CH equation (3)-(4): given $\phi^n, \phi^{n-1} \in \mathcal{C}_{\rm per}$, find $\phi^{n+1}, \mu^{n+1} \in \mathcal{C}_{\rm per}$, such that

$$\frac{\frac{3}{2}\phi^{n+1} - 2\phi^n + \frac{1}{2}\phi^{n-1}}{\Delta t} = \nabla_h \cdot (\widehat{\mathcal{M}}^{n+1} \nabla_h \mu^{n+1}), \tag{70}$$

where

$$\begin{aligned} \mu^{n+1} =& \ln(1+\phi^{n+1}) - \ln(1-\phi^{n+1}) - \theta_0 \check{\phi}^{n+1} - A\Delta t \Delta_h(\phi^{n+1} - \phi^n) - \varepsilon^2 \Delta_h \phi^{n+1}, \\ \check{\phi}^{n+1} =& 2\phi^n - \phi^{n-1}, \end{aligned} \tag{71}$$

and the discrete mobility function is defined at the face center points in a similar way as in (17): $\widehat{\mathcal{M}}^{n+1}_{i+1/2,j,k} = \mathcal{M}(A_x \check{\phi}^{n+1}_{i+1/2,j,k})$, $\widehat{\mathcal{M}}^{n+1}_{i,j+1/2,k} = \mathcal{M}(A_y \check{\phi}^{n+1}_{i,j+1/2,k})$, $\widehat{\mathcal{M}}^{n+1}_{i,j,k+1/2} = \mathcal{M}(A_z \check{\phi}^{n+1}_{i,j,k+1/2})$.

In the case of constant mobility $\mathcal{M}(\phi) \equiv 1$, the positivity-preserving property is established in the following theorem.

Theorem 6.1. *Assume that $\mathcal{M}(\phi) \equiv 1$. Given $\phi^k \in \mathcal{C}_{\rm per}$, with $\|\phi^k\|_\infty \le M$, $k = n, n-1$, for some $M > 0$, and $\left|\overline{\phi^k}\right| = \left|\overline{\phi^{n-1}}\right| < 1$, there exists a unique solution $\phi^{n+1} \in \mathcal{C}_{\rm per}$ to (70), with $\phi^{n+1} - \overline{\phi^n} \in \mathring{\mathcal{C}}_{\rm per}$ and $\|\phi^{n+1}\|_\infty < 1$.*

Proof. We follow the notations in the proof of Theorem 2.1. The numerical solution of (70) is a minimizer of the following discrete energy functional over the admissible set A_h:

$$\begin{aligned} \mathcal{J}^{n,(2)}(\phi) :=& \frac{1}{3\Delta t} \left\| \frac{3}{2}\phi - 2\phi^n + \frac{1}{2}\phi^{n-1} \right\|_{-1,h}^2 + \langle 1+\phi, \ln(1+\phi)\rangle_\Omega + \langle 1-\phi, \ln(1-\phi)\rangle_\Omega \\ &+ \frac{\varepsilon^2 + A\Delta t}{2} \|\nabla_h \phi\|_2^2 + \left\langle \phi, A\Delta t \Delta_h \phi^n - \theta_0 \check{\phi}^{n+1} \right\rangle_\Omega. \end{aligned} \tag{72}$$

Of course, $\mathcal{J}^{n,(2)}$ is strictly convex over A_h. Again, such a minimization problem is equivalent to the following transformed functional over $\mathring{A}_h$:

$$\begin{aligned} \mathcal{F}^{n,(2)}(\varphi) :=& \mathcal{J}^{n,(2)}(\varphi + \overline{\phi}_0) \\ =& \frac{1}{3\Delta t} \left\| \frac{3}{2}(\varphi + \overline{\phi}_0) - 2\phi^n + \frac{1}{2}\phi^{n-1} \right\|_{-1,h}^2 \\ &+ \left\langle 1+\varphi+\overline{\phi}_0, \ln(1+\varphi+\overline{\phi}_0)\right\rangle_\Omega + \left\langle 1-\varphi-\overline{\phi}_0, \ln(1-\varphi-\overline{\phi}_0)\right\rangle_\Omega \\ &+ \frac{\varepsilon^2 + A\Delta t}{2} \|\nabla_h \varphi\|_2^2 + \left\langle \varphi + \overline{\phi}_0, A\Delta t \Delta_h \phi^n - \theta_0 \check{\phi}^{n+1} \right\rangle_\Omega. \end{aligned} \tag{73}$$

To obtain the existence of a minimizer for $\mathcal{F}^{n,(2)}$ over $\mathring{A}_h$, we consider the closed domain $\mathring{A}_{h,\delta}$ for $0 < \delta < \frac{1}{2}$, as defined by (37). There exists a (not necessarily unique) minimizer of $\mathcal{F}^{n,(2)}$ over $\mathring{A}_{h,\delta}$, and we have to prove such a minimizer could not occur on the boundary of $\mathring{A}_{h,\delta}$, if δ is sufficiently small. To get a contradiction, suppose that the minimizer of $\mathcal{F}^{n,(2)}$, call it $\varphi^\star$ occurs at a boundary point of $\mathring{A}_{h,\delta}$. There is at least one grid point $\vec{\alpha}_0 = (i_0, j_0, k_0)$ such that $|\varphi^\star_{\vec{\alpha}_0} + \overline{\phi}_0| = 1 - \delta$. Similarly, we assume that $\varphi^\star_{\vec{\alpha}_0} + \overline{\phi}_0 = \delta - 1$, so that the grid function $\varphi^\star$ has a global minimum at $\vec{\alpha}_0$, and $\vec{\alpha}_1 = (i_1, j_1, k_1)$ is a grid point at which $\varphi^\star$ achieves its maximum. Meanwhile, for all $\psi \in \mathring{\mathcal{C}}_{\rm per}$, the directional derivative becomes

$$\begin{aligned} d_s \mathcal{F}^{n,(2)}(\varphi^\star + s\psi)|_{s=0} =& \left\langle \ln(1+\varphi^\star+\overline{\phi}_0) - \ln(1-\varphi^\star-\overline{\phi}_0), \psi \right\rangle_\Omega \\ &+ \left\langle A\Delta t \Delta_h \phi^n - \theta_0 \check{\phi}^{n+1}, \psi \right\rangle_\Omega - (\varepsilon^2 + A\Delta t) \left\langle \Delta_h \varphi^\star, \psi \right\rangle_\Omega \\ &+ \frac{1}{\Delta t} \left\langle (-\Delta_h)^{-1} \left(\frac{3}{2}(\varphi^\star + \overline{\phi}_0) - 2\phi^n + \frac{1}{2}\phi^{n-1} \right), \psi \right\rangle_\Omega. \end{aligned}$$

In more details, this derivative may be expressed as

$$\begin{aligned} \frac{1}{h^3} d_s \mathcal{F}^{n,(2)}(\varphi^\star + s\psi)|_{s=0} =& \ln(1+\varphi^\star_{\vec{\alpha}_0} + \overline{\phi}_0) - \ln(1-\varphi^\star_{\vec{\alpha}_0} - \overline{\phi}_0) - \ln(1+\varphi^\star_{\vec{\alpha}_1} + \overline{\phi}_0) + \ln(1-\varphi^\star_{\vec{\alpha}_1} - \overline{\phi}_0) \\ &- \theta_0(\check{\phi}^{n+1}_{\vec{\alpha}_0} - \check{\phi}^{n+1}_{\vec{\alpha}_1}) + A\Delta t(\Delta_h \phi^n_{\vec{\alpha}_0} - \Delta_h \phi^n_{\vec{\alpha}_1}) - (\varepsilon^2 + A\Delta t)(\Delta_h \varphi^\star_{\vec{\alpha}_0} - \Delta_h \varphi^\star_{\vec{\alpha}_1}) \end{aligned}$$

$$+\frac{1}{\Delta t}(-\Delta_h)^{-1}(\frac{3}{2}(\varphi^\star+\overline{\phi}_0)-2\phi^n+\frac{1}{2}\phi^{n-1})_{\vec{\alpha}_0}$$
$$-\frac{1}{\Delta t}(-\Delta_h)^{-1}(\frac{3}{2}(\varphi^\star+\overline{\phi}_0)-2\phi^n+\frac{1}{2}\phi^{n-1})_{\vec{\alpha}_1}. \tag{74}$$

Furthermore, the following estimates are derived

$$\Delta_h\phi^\star_{\vec{\alpha}_0}\ge 0,\quad \Delta_h\phi^\star_{\vec{\alpha}_1}\le 0, \tag{75}$$
$$-6M\le \check{\phi}^{n+1}_{\vec{\alpha}_0}-\check{\phi}^{n+1}_{\vec{\alpha}_1}\le 6M, \tag{76}$$
$$\Delta_h\phi^n_{\vec{\alpha}_0}\le\frac{12M}{h^2},\quad \Delta_h\phi^n_{\vec{\alpha}_1}\ge-\frac{12M}{h^2}, \tag{77}$$
$$-5C_1\le(-\Delta_h)^{-1}(\frac{3}{2}(\varphi^\star+\overline{\phi}_0)-2\phi^n+\frac{1}{2}\phi^{n-1})_{\vec{\alpha}_0}$$
$$-(-\Delta_h)^{-1}(\frac{3}{2}(\varphi^\star+\overline{\phi}_0)-2\phi^n+\frac{1}{2}\phi^{n-1})_{\vec{\alpha}_1}\le 5C_1, \tag{78}$$

in which we have repeatedly made use of the fact that $\|\phi^k\|_\infty\le M$, $k=n,n-1$, as well as the application of Lemma 3.1. Subsequently, a substitution of (75) – (78) and (39) into (74) yields the following bound:

$$\frac{1}{h^3}d_s\mathcal{F}^{n,(2)}(\varphi^\star+s\psi)|_{s=0}\le\ln\frac{\delta}{2-\delta}-\ln\frac{1+\overline{\phi}_0}{1-\overline{\phi}_0}+6M\theta_0+24AM\Delta t h^{-2}+10C_1\Delta t^{-1}. \tag{79}$$

The rest analysis follows the same arguments as in the proof of Theorem 2.1; the details are left to interested readers. □

Remark 6.1. Again, for the second order scheme, a careful calculation implies that $C_8=O(\Delta t^{-1}+\Delta t h^{-2})$, which becomes singular as $\Delta t,h\to 0$. Even so, since the values of h and Δt are fixed, a $\delta\in(0,1/2)$ exists so that the size of C_8 is not an issue.

The non-constant mobility case could be analyzed in the same fashion; we state the result below, and the technical details are left to interested readers.

Theorem 6.2. *Assume that $\mathcal{M}(x)\ge\mathcal{M}_0>0$, for all $x\in[-1,1]$. Given $\phi^k\in\mathcal{C}_{\rm per}$, with $\|\phi^k\|\le M$, $k=n,n-1$, for some $M>0$, and $|\overline{\phi^n}|=|\overline{\phi^{n-1}}|<1$, there exists a unique solution $\phi^{n+1}\in\mathcal{C}_{\rm per}$ to (70), with $\phi^{n+1}-\overline{\phi^n}\in\mathring{\mathcal{C}}_{\rm per}$ and $\|\phi^{n+1}\|_\infty<1$.*

In the case of constant mobility $\mathcal{M}(\phi)\equiv 1$, a modified energy stability is available for the second order BDF scheme (70), provided that $A\ge\frac{1}{16}$.

Theorem 6.3. *Suppose $\mathcal{M}(\phi)\equiv 1$. With the same assumptions as in Theorem 4.1, we have the stability analysis of the following modified energy functional for the proposed numerical scheme (70):*

$$\tilde{E}_h(\phi^{n+1},\phi^n)\le\tilde{E}_h(\phi^n,\phi^{n-1}),\quad \text{with} \tag{80}$$
$$\tilde{E}_h(\phi^{n+1},\phi^n)=E_h(\phi^{n+1})+\frac{1}{4\Delta t}\|\phi^{n+1}-\phi^n\|^2_{-1,h}+\frac{1}{2}\|\phi^{n+1}-\phi^n\|^2_2, \tag{81}$$

for any $\Delta t,h>0$, provided that $A\ge\frac{1}{16}$.

Proof. By taking an inner product with (70) by $(-\Delta_h)^{-1}(\phi^{n+1}-\phi^n)$, we could derive the following inequalities:

$$\left\langle\frac{\frac{3}{2}\phi^{n+1}-2\phi^n+\frac{1}{2}\phi^{n-1}}{\Delta t},(-\Delta_h)^{-1}(\phi^{n+1}-\phi^n)\right\rangle_\Omega$$
$$=\frac{3}{2\Delta t}\|\phi^{n+1}-\phi^n\|^2_{-1,h}-\frac{1}{2}\langle\phi^{n+1}-\phi^n,\phi^n-\phi^{n-1}\rangle_{-1,h}$$
$$\ge\frac{1}{\Delta t}\left(\frac{5}{4}\|\phi^{n+1}-\phi^n\|^2_{-1,h}-\frac{1}{4}\|\phi^n-\phi^{n-1}\|^2_{-1,h}\right), \tag{82}$$
$$\left\langle-\Delta_h(\ln(1+\phi^{n+1})),(-\Delta_h)^{-1}(\phi^{n+1}-\phi^n)\right\rangle_\Omega=\left\langle\ln(1+\phi^{n+1}),\phi^{n+1}-\phi^n\right\rangle_\Omega$$
$$\ge\left\langle 1+\phi^{n+1},\ln(1+\phi^{n+1})\right\rangle_\Omega-\left\langle 1+\phi^n,\ln(1+\phi^n)\right\rangle_\Omega, \tag{83}$$

$$\left\langle \Delta_h(\ln(1-\phi^{n+1})), (-\Delta_h)^{-1}(\phi^{n+1}-\phi^n)\right\rangle_\Omega = -\left\langle \ln(1-\phi^{n+1}), \phi^{n+1}-\phi^n\right\rangle_\Omega$$
$$\geq -\left\langle 1-\phi^{n+1}, \ln(1-\phi^{n+1})\right\rangle_\Omega + \left\langle 1-\phi^n, \ln(1-\phi^n)\right\rangle_\Omega, \tag{84}$$
$$\left\langle \Delta_h^2\phi^{n+1}, (-\Delta_h)^{-1}(\phi^{n+1}-\phi^n)\right\rangle_\Omega = \left\langle \nabla_h\phi^{n+1}, \nabla_h(\phi^{n+1}-\phi^n)\right\rangle_\Omega$$
$$= \frac{1}{2}\left(\|\nabla_h\phi^{n+1}\|_2^2 - \|\nabla_h\phi^n\|_2^2 + \|\nabla_h(\phi^{n+1}-\phi^n)\|_2^2\right), \tag{85}$$
$$\Delta t\left\langle \Delta_h^2(\phi^{n+1}-\phi^n), (-\Delta_h)^{-1}(\phi^{n+1}-\phi^n)\right\rangle_\Omega = \Delta t\|\nabla_h(\phi^{n+1}-\phi^n)\|_2^2, \tag{86}$$
$$\left\langle \Delta_h(2\phi^n-\phi^{n-1}), (-\Delta_h)^{-1}(\phi^{n+1}-\phi^n)\right\rangle_\Omega = -\left\langle 2\phi^n-\phi^{n-1}, \phi^{n+1}-\phi^n\right\rangle_\Omega$$
$$\geq -\frac{1}{2}\left(\|\phi^{n+1}\|_2^2 - \|\phi^n\|_2^2\right) - \frac{1}{2}\|\phi^n-\phi^{n-1}\|_2^2, \tag{87}$$

in which (83), (84) are based on the convexity of $(1+\phi)\ln(1+\phi)$, $(1-\phi)\ln(1-\phi)$, respectively. Meanwhile, an application of Cauchy inequality indicates the following estimate:

$$\frac{1}{\Delta t}\|\phi^{n+1}-\phi^n\|_{-1,h}^2 + A\Delta t\|\nabla_h(\phi^{n+1}-\phi^n)\|_2^2 \geq 2A^{1/2}\|\phi^{n+1}-\phi^n\|_2^2. \tag{88}$$

Therefore, a combination of (82)-(87) and (88) yields

$$E_h(\phi^{n+1}) - E_h(\phi^n) + \frac{1}{4\Delta t}\left(\|\phi^{n+1}-\phi^n\|_{-1,h}^2 - \|\phi^n-\phi^{n-1}\|_{-1,h}^2\right)$$
$$+\frac{1}{2}\left(\|\phi^{n+1}-\phi^n\|_2^2 - \|\phi^n-\phi^{n-1}\|_2^2\right) \leq (-2A^{1/2}+\frac{1}{2})\|\phi^{n+1}-\phi^n\|_2^2 \leq 0, \tag{89}$$

provided that $A \geq \frac{1}{16}$. Therefore, by denoting a modified energy as given by (81), we get the energy estimate (80). This completes the proof of Theorem 6.3. □

With the same assumption that $\mathcal{M}(\phi)\equiv 1$, the convergence result is stated in the following theorem.

Theorem 6.4. *Given initial data $\Phi(\cdot, t=0) \in C^6_{\text{per}}(\Omega)$, suppose the exact solution for Cahn-Hilliard equation (3)-(4) is of regularity class $\mathcal{R}_2 := H^3\left(0, T; C_{\text{per}}(\Omega)\right) \cap H^3\left(0, T; C^2_{\text{per}}(\Omega)\right) \cap L^\infty\left(0, T; C^6_{\text{per}}(\Omega)\right)$. Then, provided Δt and h are sufficiently small, for all positive integers n, such that $t_n \leq T$, we have the following convergence estimate for the numerical solution (70)*

$$\|\tilde{\phi}^n\|_{-1,h} + \left(\varepsilon^2\Delta t\sum_{m=1}^n \|\nabla_h\tilde{\phi}^m\|_2^2\right)^{1/2} \leq C(\Delta t^2 + h^2), \tag{90}$$

where $C>0$ is independent of n, Δt, and h.

Proof. A careful consistency analysis indicates the following truncation error estimate:

$$\frac{\frac{3}{2}\Phi_N^{n+1} - 2\Phi_N^n + \frac{1}{2}\Phi_N^{n-1}}{\Delta t} = \Delta_h\Big(\ln(1+\Phi_N^{n+1}) - \ln(1-\Phi_N^{n+1}) - \theta_0\check{\Phi}_N^{n+1} - \varepsilon^2\Delta_h\Phi_N^{n+1}$$
$$- A\Delta t\Delta_h(\Phi_N^{n+1}-\Phi_N^n)\Big) + \tau^n, \tag{91}$$

with $\check{\Phi}_N^n = 2\Phi_N^n - \Phi_N^{n-1}$, $\|\tau^n\|_{-1,h} \leq C(\Delta t^2+h^2)$. In turn, subtracting the numerical scheme (70) from (60) gives

$$\frac{\frac{3}{2}\tilde{\phi}^{n+1} - 2\tilde{\phi}^n + \frac{1}{2}\tilde{\phi}^{n-1}}{\Delta t} = \Delta_h\Big((\ln(1+\Phi_N^{n+1}) - \ln(1+\phi^{n+1})) - (\ln(1-\Phi_N^{n+1}) - \ln(1-\phi^{n+1})) - \theta_0\tilde{\check{\phi}}^{n+1}$$
$$- \varepsilon^2\Delta_h\tilde{\phi}^{n+1} - A\Delta t\Delta_h(\tilde{\phi}^{n+1}-\tilde{\phi}^n)\Big) + \tau^n, \tag{92}$$

with $\tilde{\check{\phi}}^{n+1} = 2\tilde{\phi}^n - \tilde{\phi}^{n-1}$. Taking a discrete inner product with (92) by $2(-\Delta_h)^{-1}\tilde{\phi}^{n+1}$ yields

$$\left\langle 3\tilde{\phi}^{n+1} - 4\tilde{\phi}^n + \tilde{\phi}^{n-1}, \tilde{\phi}^{n+1}\right\rangle_{-1,h} - 2\varepsilon^2\Delta t\left\langle \tilde{\phi}^{n+1}, \Delta_h\tilde{\phi}^{n+1}\right\rangle_\Omega$$
$$+2\Delta t\left\langle \ln(1+\Phi_N^{n+1}) - \ln(1+\phi^{n+1}), \tilde{\phi}^{n+1}\right\rangle_\Omega$$
$$-2\Delta t\left\langle \ln(1-\Phi_N^{n+1}) - \ln(1-\phi^{n+1}), \tilde{\phi}^{n+1}\right\rangle_\Omega$$
$$-2A\Delta t\langle\Delta_h(\tilde{\phi}^{n+1}-\tilde{\phi}^n), \tilde{\phi}^{n+1}\rangle_\Omega = 2\theta_0\Delta t\left\langle \tilde{\check{\phi}}^{n+1}, \tilde{\phi}^{n+1}\right\rangle_\Omega + 2\Delta t\langle\tau^n, \tilde{\phi}^{n+1}\rangle_{-1,h}. \tag{93}$$

For the temporal derivative stencil, the following identity is valid:

$$\begin{aligned}&\left\langle 3\tilde{\phi}^{n+1}-4\tilde{\phi}^{n}+\tilde{\phi}^{n-1},\tilde{\phi}^{n+1}\right\rangle_{-1,h}\\&=\frac{1}{2}\Big(\|\tilde{\phi}^{n+1}\|_{-1,h}^2-\|\tilde{\phi}^{n}\|_{-1,h}^2+\|2\tilde{\phi}^{n+1}-\tilde{\phi}^{n}\|_{-1,h}^2-\|2\tilde{\phi}^{n}-\tilde{\phi}^{n-1}\|_{-1,h}^2+\|\tilde{\phi}^{n+1}-2\tilde{\phi}^{n}+\tilde{\phi}^{n-1}\|_{-1,h}^2\Big).\end{aligned}\tag{94}$$

The estimates for the terms associated with the surface diffusion, the nonlinear product and the truncation error follow exactly the same way as in (63), (64), (65), (67), respectively. For the concave expansive error term, a similar inequality is available:

$$\begin{aligned}2\theta_0\left\langle\tilde{\tilde{\phi}}^{n+1},\tilde{\phi}^{n+1}\right\rangle_{\Omega}&\le 2\theta_0\|\tilde{\tilde{\phi}}^{n+1}\|_{-1,h}\|\nabla_h\tilde{\phi}^{n+1}\|_2\le\theta_0^2\varepsilon^{-2}\|\tilde{\tilde{\phi}}^{n+1}\|_{-1,h}^2+\varepsilon^2\|\nabla_h\tilde{\phi}^{n+1}\|_2\\&\le\theta_0^2\varepsilon^{-2}(8\|\tilde{\phi}^{n}\|_{-1,h}^2+2\|\tilde{\phi}^{n-1}\|_{-1,h}^2)+\varepsilon^2\|\nabla_h\tilde{\phi}^{n+1}\|_2.\end{aligned}\tag{95}$$

In addition, the following identity could be derived for the artificial diffusion term:

$$\begin{aligned}&-2\langle\Delta_h(\tilde{\phi}^{n+1}-\tilde{\phi}^{n}),\tilde{\phi}^{n+1}\rangle_{\Omega}=2\langle\nabla_h(\tilde{\phi}^{n+1}-\tilde{\phi}^{n}),\nabla_h\tilde{\phi}^{n+1}\rangle_{\Omega}\\&=\|\nabla_h\tilde{\phi}^{n+1}\|_2^2-\|\nabla_h\tilde{\phi}^{n}\|_2^2+\|\nabla_h(\tilde{\phi}^{n+1}-\tilde{\phi}^{n})\|_2^2.\end{aligned}\tag{96}$$

Subsequently, a substitution of (94) – (96), (63), (64), (65) and (67) into (93) yields

$$\begin{aligned}&\|\tilde{\phi}^{n+1}\|_{-1,h}^2-\|\tilde{\phi}^{n}\|_{-1,h}^2+\|2\tilde{\phi}^{n+1}-\tilde{\phi}^{n}\|_{-1,h}^2-\|2\tilde{\phi}^{n}-\tilde{\phi}^{n-1}\|_{-1,h}^2\\&+A\Delta t(\|\nabla_h\tilde{\phi}^{n+1}\|_2^2-\|\nabla_h\tilde{\phi}^{n}\|_2^2)+\varepsilon^2\Delta t\|\nabla_h\tilde{\phi}^{n+1}\|_2^2\\&\le 4\theta_0^2\varepsilon^{-2}(4\|\tilde{\phi}^{n}\|_{-1,h}^2+\|\tilde{\phi}^{n-1}\|_{-1,h}^2)+2\Delta t\|\tau^{n}\|_{-1,h}^2.\end{aligned}\tag{97}$$

Finally, an application of a discrete Gronwall inequality results in the desired convergence estimate:

$$\|\tilde{\phi}^{n+1}\|_{-1,h}+\left(\varepsilon^2\Delta t\sum_{k=0}^{n+1}\|\nabla_h\tilde{\phi}^{m}\|_2^2\right)^{1/2}\le C(\Delta t^2+h^2),\tag{98}$$

where $C>0$ is independent of Δt, h, and n. This completes the proof of the Theorem 6.4. □

Remark 6.2. Other than the modified BDF2 temporal stencil, there have been other second order accurate, energy stable approaches for the Cahn-Hilliard equation, such as the modified Crank-Nicolson approximation, which has been successfully applied to the one (7) with polynomial approximation [28,29,44,45]. On the other hand, for the equation with Flory-Huggins energy potential, the positivity-preserving, energy stability analysis and the convergence estimates for the corresponding Crank-Nicolson approximation are expected to be much more challenging than the BDF2 algorithm, due to the singular nature of the logarithmic terms. This analysis will be left to the future works.

Remark 6.3. In the optimal rate convergence estimates for both the first and second order accurate schemes, given by Theorems 5.1, 6.4, respectively, a technical assumption of a constant mobility, i.e., $\mathcal{M}\equiv\mathcal{M}_0$, has been made to simplify the analysis details. For a non-constant mobility case, the convergence estimates are expected to be much more challenging, since a direct H_h^{-1} analysis is not applicable any more. Much more complicated techniques, such as a combination of rough error estimate (to obtain a phase separation property for the numerical solution) and refined error estimate, have to be applied. These technical details will be reported in future works.

7. Numerical results

In this section we describe a simple multigrid solver for the proposed schemes, and we provided some tests that show the efficiency of the solver and the accuracy of the scheme. We demonstrate, in particular, the positivity of the solutions to the proposed Cahn-Hilliard scheme.

For the discussion of the numerical computations, we use a slightly different formulation of the Cahn-Hilliard equation, one that allows for a comparison with the so-called obstacle potential. Specifically, we will use the standard Ginzburg-Landau free energy $E[\phi]=\int_\Omega\left\{f(\phi)+\frac{\varepsilon^2}{2}|\nabla\phi|^2\right\}d\mathbf{x}$, where $f(\phi)=f_c(\phi)-f_e(\phi)$ and

$$f_c(\phi)=\frac{1}{2\theta_0}\left[(1-\phi)\ln(1-\phi)+(1+\phi)\ln(1+\phi)\right],\quad f_e(\phi)=\frac{1}{2}(\phi-1)(\phi+1).$$

Importantly, as $\theta_0\to\infty$, f tends to the obstacle potential

$$f_{\text{obs}}(\theta) = \begin{cases} \frac{1}{2}(\phi-1)(\phi+1) & \text{if} \quad -1 < \phi < 1 \\ \infty & \text{if} \quad |\phi| \geq 1, \end{cases}$$

which has been investigated elsewhere [13,14]. While we are only interested in the case of finite values of θ_0, it is interesting to explore the effects of increasing θ_0. For finite θ_0, clearly $f_e'(\phi) = \phi$ and

$$f_c'(\phi) = \frac{1}{2\theta_0}\left[\ln(1+\phi) - \ln(1-\phi)\right].$$

The Cahn-Hillard equation still takes the form (3), but with the chemical potential expressed as

$$\mu = f_c'(\phi) - f_e'(\phi) - \varepsilon^2 \Delta \phi.$$

As before, we assume that the mobility satisfies $\mathcal{M}(x) \geq \mathcal{M}_0 > 0$, for all $x \in [-1, 1]$, for some $\mathcal{M}_0$, though as we have remarked, this can be relaxed.

7.1. Multigrid solver

In this subsection, we describe a nonlinear full approximation storage (FAS) multigrid solver for the convex-concave decomposition scheme for the Cahn-Hilliard equation with logarithmic potential. The solver for the Allen-Cahn equation is simpler, and we omit its description. Our solver is similar in style to the one presented in [47], and it can be extended to the case of multi-component systems as in [25]. For an alternative approach to the one taken here and in [47], see, for example, [40].

For our solver implementation, we will need to regularize f_c'. This is due to the fact that our multigrid solver is not designed to guarantee the boundedness of the solution for arbitrary multigrid iterations, as we discuss below. Our solver will, however, converge to the correct bounded solution, provided the regularization is sufficiently small. We show this in our tests.

To effect the desired regularization, we modify the logarithm as follows: for a given $\delta \in (0, 1/4)$ we define

$$\ln_\delta(\phi) = \begin{cases} \ln(\phi) & \text{if } \delta < \phi \\ \ln(\delta) + \frac{\phi - \delta}{\delta} & \text{if } \phi \leq \delta. \end{cases}$$

The regularized logarithm, $\ln_\delta$ is defined for all values of ϕ. Using this function, we define

$$f_{c,\delta}'(\phi) = \frac{1}{2\theta_0}\left[\ln_\delta(1+\phi) - \ln_\delta(1-\phi)\right].$$

We then observe that $f_c'(\phi) = f_{c,\delta}'(\phi)$, for all $-1+\delta \leq \phi \leq 1-\delta$. Consequently, we can always take the value of δ to be small enough such that the theoretical solution to our scheme lies in this range of equivalence.

The first-order convex-concave decomposition (CS1) scheme (15) in 2-D is equivalent to the following: find $\phi, \mu \in \mathcal{C}_{\text{per}}$ whose components satisfy

$$\phi_{i,j} - \Delta t\, d_x\left(\mathcal{M}\left(A_x\phi^m\right) D_x\mu\right)_{i,j} - \Delta t\, d_y\left(\mathcal{M}\left(A_y\phi^m\right) D_y\mu\right)_{i,j} = \phi_{i,j}^m, \tag{99}$$

$$\mu_{i,j} - f_{c,\delta}'\left(\phi_{i,j}\right) + \varepsilon^2 \Delta_h \phi_{i,j} = -\phi_{i,j}^m, \tag{100}$$

where we have dropped the time superscripts $m+1$ on the unknowns. The 3-D equations are similar, and they are omitted for simplicity. For the sake of comparison, the standard backward Euler scheme (BE) is

$$\phi_{i,j} - \Delta t\, d_x\left(\mathcal{M}\left(A_x\phi\right) D_x\mu\right)_{i,j} - \Delta t\, d_y\left(\mathcal{M}\left(A_y\phi\right) D_y\mu\right)_{i,j} = \phi_{i,j}^m, \tag{101}$$

$$\mu_{i,j} - f_{c,\delta}'\left(\phi_{i,j}\right) + \phi_{i,j} + \varepsilon^2 \Delta_h \phi_{i,j} = 0. \tag{102}$$

We note that, for solvability and stability considerations, the sign of the linear term $+\phi_{i,j}$ in the chemical potential equation (102) is problematical. However, this scheme is solvable with a mild time step restriction.

The energy stable BDF2 (BDF2_ES) scheme (70) is expressed in 2D as

$$\phi_{i,j} - \frac{2\Delta t}{3} d_x\left(\mathcal{M}\left(A_x\check{\phi}^{m+1}\right) D_x\mu\right)_{i,j} - \frac{2\Delta t}{3} d_y\left(\mathcal{M}\left(A_y\check{\phi}^{m+1}\right) D_y\mu\right)_{i,j} = \frac{4}{3}\phi_{i,j}^m - \frac{1}{3}\phi_{i,j}^{m-1}, \tag{103}$$

$$\mu_{i,j} - f_{c,\delta}'\left(\phi_{i,j}\right) + \varepsilon^2 \Delta_h \phi_{i,j} + A\Delta t \Delta_h \phi_{i,j} = A\Delta t \Delta_h \phi_{i,j}^m - \check{\phi}_{i,j}^{m+1}, \tag{104}$$

where

$$\check{\phi}_{i,j}^{m+1} = 2\phi_{i,j}^m - \phi_{i,j}^{m-1}.$$

The standard BDF2 scheme is

$$\phi_{i,j} - \frac{2\Delta t}{3} d_x \left(\mathcal{M}\left(A_x\phi\right) D_x\mu\right)_{i,j} - \frac{2\Delta t}{3} d_y \left(\mathcal{M}\left(A_y\phi\right) D_y\mu\right)_{i,j} = \frac{4}{3}\phi^m_{i,j} - \frac{1}{3}\phi^{m-1}_{i,j}, \tag{105}$$

$$\mu_{i,j} - f'_{c,\delta}\left(\phi_{i,j}\right) + \phi_{i,j} + \varepsilon^2 \Delta_h \phi_{i,j} = 0. \tag{106}$$

As for the backward Euler scheme, solvability and stability are not unconditionally guaranteed for this scheme.

We use a nonlinear FAS multigrid method to solve all of the schemes efficiently. We give the details only for the (CS1) scheme, equations (99) – (100). The details for the other methods are quite similar. Our solver requires defining operator and source terms, which we do as follows. Let $\boldsymbol{\phi} = (\phi, \mu)^T$. Define the nonlinear operator $\mathbf{N} = (N^{(1)}, N^{(2)})^T$ as

$$N^{(1)}_{i,j}\left(\boldsymbol{\phi}\right) = \phi_{i,j} - \Delta t\, d_x \left(M\left(A_x\phi^m\right) D_x\mu\right)_{i,j} - \Delta t\, d_y \left(M\left(A_y\phi^m\right) D_y\mu\right)_{i,j}, \tag{107}$$

$$N^{(2)}_{i,j}\left(\boldsymbol{\phi}\right) = \mu_{i,j} - f'_{c,\delta}\left(\phi_{i,j}\right) + \varepsilon^2 \Delta_h \phi_{i,j}, \tag{108}$$

and the source $\mathbf{S} = (S^{(1)}, S^{(2)})^T$ as

$$S^{(1)}_{i,j}\left(\boldsymbol{\phi}\right) = \phi_{i,j}, \qquad S^{(2)}_{i,j}\left(\boldsymbol{\phi}\right) = -\phi_{i,j}. \tag{109}$$

Then, of course, Equations (99) – (100) are equivalent to $\mathbf{N}(\boldsymbol{\phi}^{m+1}) = \mathbf{S}(\boldsymbol{\phi}^m)$. Notice that the operator $\mathbf{N}$ depends upon the time step m, because its definition involves the solution ϕ^m.

We mention that for the backward Euler (BE) scheme, the only difference in this decomposition is that

$$N^{(2)}_{i,j}\left(\boldsymbol{\phi}\right) = \mu_{i,j} - f'_{c,\delta}\left(\phi_{i,j}\right) + \phi_{i,j} + \varepsilon^2 \Delta_h \phi_{i,j}, \quad S^{(2)}_{i,j}\left(\boldsymbol{\phi}\right) = 0.$$

The BDF2_ES and BDF2 schemes are handled using similar considerations.

We will describe a somewhat standard nonlinear FAS multigrid scheme for solving the vector equation $\mathbf{N}(\boldsymbol{\phi}^{m+1}) = \mathbf{S}(\boldsymbol{\phi}^m)$. Here we will sketch only the important points of the algorithm; the reader is referred to Trottenberg et al. [60, Sec. 5.3] and our paper [63] for complete details. For this issue, we need to discuss a smoothing operator for generating *smoothed* approximate solutions of $\mathbf{N}(\boldsymbol{\phi}) = \mathbf{S}$. The action of this operator is represented as

$$\widetilde{\boldsymbol{\phi}} = \text{Smooth}\left(\lambda, \boldsymbol{\phi}, \mathbf{N}, \mathbf{S}\right), \tag{110}$$

where $\boldsymbol{\phi}$ is an approximate solution prior to smoothing, $\bar{\boldsymbol{\phi}}$ is the smoothed approximation, and λ is the number of smoothing sweeps. For smoothing we use a nonlinear Gauss-Seidel method with Red-Black ordering. In what follows, to simplify the discussion, we give the details of the relaxation using the simpler lexicographic ordering. Let ℓ be the index for the lexicographic Gauss-Seidel. (Note that the smoothing index ℓ in the following should not be confused with the time step index m.) Now we set

$$M^{\text{ew}}_{i+1/2,j} := \mathcal{M}\left(A_x\phi^m_{i+1/2,j}\right), \qquad M^{\text{ns}}_{i,j+1/2} := \mathcal{M}\left(A_y\phi^m_{i,j+1/2}\right).$$

The Gauss-Seidel smoothing is as follows: for every (i, j), stepping lexicographically from $(1, 1)$ to (N, N), find $\phi^{\ell+1}_{i,j}$, and $\mu^{\ell+1}_{i,j}$ that solve

$$\begin{aligned}
&\phi^{\ell+1}_{i,j} + \frac{\Delta t}{h^2}\left(M^{\text{ew}}_{i+1/2,j} + M^{\text{ew}}_{i-1/2,j} + M^{\text{ns}}_{i,j+1/2} + M^{\text{ns}}_{i,j-1/2}\right)\mu^{\ell+1}_{i,j} \\
&\quad = S^{(1)}_{i,j}\left(\boldsymbol{\phi}^m\right) + \frac{\Delta t}{h^2}\left(M^{\text{ew}}_{i+1/2,j}\mu^{\ell}_{i+1,j} + M^{\text{ew}}_{i-1/2,j}\mu^{\ell+1}_{i-1,j} + M^{\text{ns}}_{i,j+1/2}\mu^{\ell}_{i,j+1} + M^{\text{ns}}_{i,j-1/2}\mu^{\ell+1}_{i,j-1}\right),
\end{aligned} \tag{111}$$

$$\begin{aligned}
&\left(-f''_{c,\delta}\left(\phi^{\ell}_{i,j}\right) - \frac{4\varepsilon^2}{h^2}\right)\phi^{\ell+1}_{i,j} + \mu^{\ell+1}_{i,j} \\
&\quad = S^{(2)}_{i,j}\left(\boldsymbol{\phi}^m\right) + f'_{c,\delta}\left(\phi^{\ell}_{i,j}\right) - \phi^{\ell}_{i,j} f''_{c,\delta}\left(\phi^{\ell}_{i,j}\right) - \frac{\varepsilon^2}{h^2}\left(\phi^{\ell}_{i+1,j} + \phi^{\ell+1}_{i-1,j} + \phi^{\ell}_{i,j+1} + \phi^{\ell+1}_{i,j-1}\right).
\end{aligned} \tag{112}$$

Note that we have linearized the logarithmic term using a local Newton approximation, but otherwise this is a standard vector application of block Gauss-Seidel. The 2×2 linear system defined by (111) – (112) is unconditionally solvable (the determinant of the coefficient matrix is always positive in this case). We use Cramer's Rule to obtain $\phi^{\ell+1}_{i,j}$ and $\mu^{\ell+1}_{i,j}$. However, we observe that it is not guaranteed that $-1 < \phi^{\ell+1}_{i,j} < 1$ for an arbitrary smoothing step.

The only difference for the backward Euler (BE) scheme is that second equation (112) in the block smoother is replaced by

$$\begin{aligned}
&\left(-f''_{c,\delta}\left(\phi^{\ell}_{i,j}\right) - \frac{4\varepsilon^2}{h^2}\right)\phi^{\ell+1}_{i,j} + \mu^{\ell+1}_{i,j} \\
&\quad = S^{(2)}_{i,j}\left(\boldsymbol{\phi}^m\right) + f'_{c,\delta}\left(\phi^{\ell}_{i,j}\right) - \phi^{\ell}_{i,j} - \phi^{\ell}_{i,j} f''_{c,\delta}\left(\phi^{\ell}_{i,j}\right) - \frac{\varepsilon^2}{h^2}\left(\phi^{\ell}_{i+1,j} + \phi^{\ell+1}_{i-1,j} + \phi^{\ell}_{i,j+1} + \phi^{\ell+1}_{i,j-1}\right).
\end{aligned}$$

Table 1
Maximum and minimum values of $\phi^k_{i,j}$ during spinodal decomposition, computed using the first-order convex-concave decomposition (CS1) scheme. The common parameters are $\varepsilon = 5.0 \times 10^{-3}$, $T = 1.0$, $L = 1.0$, $h = 1/256$, $\Delta t = 1.0 \times 10^{-3}$, $\tau = 1.0 \times 10^{-9}$. The initial conditions are $\phi^0_{i,j} = 0.2 + r_{i,j}$, where $r_{i,j} \in [-0.05, 0.05]$ is a uniformly distributed random variable. As θ_0 becomes larger, the potential f approaches the so-called obstacle potential, and the maxima and minima approach $+1$ and -1, respectively. But, observe that the computed values stay well within the range $(-1+\delta, 1-\delta)$.

θ_0	δ	λ	$\max_{i,j,k} \phi^k_{i,j}$	$\min_{i,j,k} \phi^k_{i,j}$
2.0	1.0×10^{-3}	2	0.958159539817000	−0.969040263101000
2.5	1.0×10^{-3}	2	0.986118743476000	−0.990903230905000
3.0	1.0×10^{-3}	2	0.995203610902000	−0.997255351479000
3.0	1.0×10^{-5}	2	0.995203610606000	−0.997255351459000
3.2	1.0×10^{-5}	3	0.996851091247000	−0.998305411243000
3.5	1.0×10^{-5}	3	0.998298616883000	−0.999144402772000

One full block Gauss-Seidel sweep has concluded when we have stepped lexicographically through all the grid points, from $(1, 1)$ to (N, N). When λ full smoothing sweeps has completed the vector result is labeled $\widetilde{\boldsymbol{\phi}}$, as in Eq. (110), and the action of the smoothing operator in (110) is complete.

Multigrid works on a hierarchy of grids. We denote the grid level by the index n, where $n_{\min} \le n \le n_{\max}$, $n_{\max}$ is the index for the finest grid, and $n_{\min}$ is the index for the coarsest grid. We need operators for communicating information from coarse levels to fine levels, and *vice versa*. By $\mathbf{I}^{n-1}_n$ we denote the restriction operator, which transfers fine grid functions, with grid index n, to the coarse grid, indexed by $n-1$. By $\mathbf{I}^n_{n-1}$ we denote the prolongation operator, which transfers coarse grid functions (level $n-1$) to the fine grid (level n). Here we work on cell-centered grids. The restriction operator is defined by cell-center averaging; for the prolongation operator we use piece-wise constant interpolation [60, Sec. 2.8.4]. The rest of the details of the nonlinear multigrid solver are similar to those given in [63]. The details are omitted for the sake of brevity.

7.2. Regularization of the logarithm in the multigrid solver

We now give a very brief discussion on how to choose the regularization parameter δ for the logarithm in the CS1 scheme. The regularization parameter must be chosen small enough so that the computed numerical solutions satisfy $-1 + \delta < \phi^m_{i,j} < 1 - \delta$, for any i, j, m. To understand the issue, consider the following simulation set-up: the common parameters are taken to be $\varepsilon = 5.0 \times 10^{-3}$, $\mathcal{M} \equiv 1$, $T = 1.0$, $L = 1.0$, $h = 1/256$, $\Delta t = 1.0 \times 10^{-3}$, $\tau = 1.0 \times 10^{-9}$ (multigrid stopping tolerance). The initial conditions are $\phi^0_{i,j} = 0.2 + r_{i,j}$, where $r_{i,j} \in [-0.05, 0.05]$ is a uniformly distributed random variable. We choose various values of the quench parameter θ_0, the smallest being $\theta_0 = 2.0$ and the largest, $\theta_0 = 3.5$. As $\theta_0 \to \infty$, the maxima and minima will tend to 1 and -1, respectively, as the singular potential approaches the obstacle potential.

We compute the maxima and minima of $\phi^m_{i,j}$ and report the values in Table 1. Observe that for modest values of θ_0, $\delta \in (0, 1)$ can always be chosen so that $\|\phi^m\|_\infty < 1 - \delta$. We point out, in particular, the case for which $\theta_0 = 3.0$. We have taken two different values of δ, 1.0×10^{-3} and 1.0×10^{-5}. The computed solutions – as well as the energies (not shown), which are decreasing at each time step – for these two cases are the same up to round-off errors.

To be safe, in all of the computed solutions that follow, we use the smaller regularization parameter $\delta = 1.0 \times 10^{-5}$. The same considerations are applied when picking the regularization parameter for 3-D simulations. In Fig. 1, we show spinodal decomposition simulation using the parameters given in the caption. For δ sufficiently small, the computed solution stays well inside the interval $(-1 + \delta, 1 - \delta)$.

In Table 2 the maximum and minimum values of $\phi^k_{i,j}$ for a simulation of spinodal decomposition and coarsening are displayed; the approximate solution is computed using the energy stable BDF2 (BDF2_ES) scheme using increasingly larger time step sizes, Δt, and stabilization parameter $A = \frac{1}{16}$. The parameters are $\varepsilon = 5.0 \times 10^{-3}$, $T = 0.1$, $L = 0.5$, $h = 0.5/512$, $\tau = 1.0 \times 10^{-10}$. The initial conditions are smooth, pictured in Fig. 3 ($t = 0$). The quench parameter is fixed at $\theta_0 = 3.0$ and the log regularization parameter is fixed as $\delta = 1.0 \times 10^{-5}$. Here the spatial grid size $h = 0.5/512$ is taken to be very small, so that there is little spatial error. The computed solution using the smallest time step size $\Delta t = 1.0 \times 10^{-6}$ is shown in Fig. 3. The energy plots are shown in Fig. 4. As the time step size Δt is made larger, the max and min values approach ± 1, respectively. This clearly shows that there is a dependence of the max and min values on the step size, Δt. Furthermore, for larger step sizes, the regularization $\delta = 1.0 \times 10^{-5}$, becomes more restrictive, in the sense that the approximate solutions become dangerously close to $1 - \delta$ and $-1 + \delta$. On the other hand, large step sizes yield solutions that are very inaccurate, as is seen in Fig. 4. This suggest that one should be careful tuning in selecting the regularization parameter δ, the same care that one would take in choosing the time step size Δt.

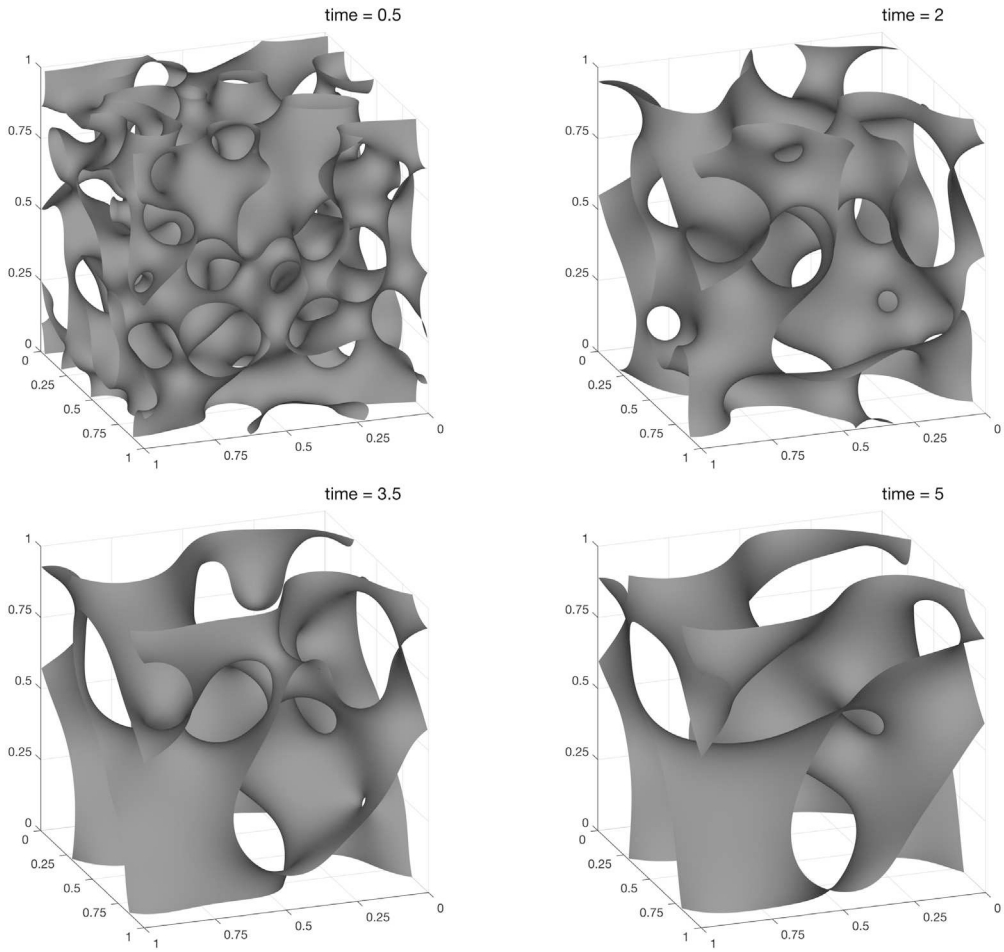

Fig. 1. Three-dimensional simulation. The parameters are $L = L_x = L_y = L_z = 1.0$; $\varepsilon = 5 \times 10^{-3}$; $\theta_0 = 3.0$; $\delta = 10^{-5}$; $T = 5.0$; $\tau = 10^{-8}$; $\Delta t = 10^{-3}$, $h = \frac{1}{256}$. For initial data, $\phi^0_{i,j,k} = r_{i,j,k}$, where $r_{i,j,k}$ is a uniformly distributed random variable from the interval $[-0.05, 0.05]$. The computed solution stays in the interval $[-0.996, 0.996]$, well inside the interval $(-1+\delta, 1-\delta)$. This computation is done using the first-order convex-concave decomposition (CS1) scheme.

Table 2
Maximum and minimum values of $\phi^k_{i,j}$ during spinodal decomposition and coarsening, computed using the energy stable BDF2 (BDF2_ES) scheme using increasingly larger time step sizes, Δt, and the stabilization parameter $A = \frac{1}{16}$. The common parameters are $\varepsilon = 5.0 \times 10^{-3}$, $T = 0.1$, $L = 0.5$, $h = 0.5/512$, $\tau = 1.0 \times 10^{-10}$. The initial conditions are smooth, pictured in Fig. 3 ($t = 0$). The quench parameter is fixed at $\theta_0 = 3.0$ and the log regularization parameter is fixed as $\delta = 1.0 \times 10^{-5}$. Here the spatial grid size $h = 0.5/512$ is taken to be very small, so that there is little spatial error. As the time step size Δt is made larger, the max and min values approach ± 1, respectively.

θ_0	δ	Δt	$\max_{i,j,k} \phi^k_{i,j}$	$\min_{i,j,k} \phi^k_{i,j}$
3.0	1.0×10^{-5}	1.0×10^{-6}	0.997502697800000	−0.998561963283000
3.0	1.0×10^{-5}	1.0×10^{-5}	0.997471083392000	−0.998558057216000
3.0	1.0×10^{-5}	1.0×10^{-4}	0.998607967114000	−0.998833800688000
3.0	1.0×10^{-5}	2.0×10^{-4}	0.999561816773000	−0.999598715832000
3.0	1.0×10^{-5}	1.0×10^{-3}	0.999906241590000	−0.999978093053000

7.3. Asymptotic ($\Delta t, h \to 0$) convergence test

Here we give a convergence test for the first-order convex-concave decomposition (CS1) scheme method and the second-order energy stable scheme (BDF2_ES) in 2-D. The initial condition for our convergence test is given by

$$\phi(x, y, 0) = 1.8 \left(\frac{1 - \cos\left(\frac{4x\pi}{3.2}\right)}{2} \right) \left(\frac{1 - \cos\left(\frac{2y\pi}{3.2}\right)}{2} \right) - 0.9. \tag{113}$$

Table 3
Errors and convergence rates for the first-order CS1 and second-order BDF2_ES schemes. The parameters are (domain size) $L = L_x = L_y = 3.2$; (interfacial parameter) $\varepsilon = 0.2$; (mobility) $\mathcal{M} \equiv 1$; (quench parameter) $\theta_0 = 3.0$; (ln regularization parameter) $\delta = 10^{-5}$; (final time) $T = 0.4$; (solver stopping tolerance) $\tau = 10^{-10}$; (stabilization parameter for BFD2_ES) $A = \frac{1}{16}$ and $A = 0$. The refinement path for the first-order CS1 scheme is quadratic, $\Delta t = 0.4h^2$, and the refinement path for the second-order BDF2_ES scheme is linear, $\Delta t = 0.8h$. The test results confirm the predicted accuracy: first order in time and second order in space for CS1 and fully second order for the BDF2_CS scheme. When $A = 0$, the BDF2_ES scheme is not provably energy dissipative, but it typically performs well and has a smaller error compared to when $A > 0$.

		CS1		BDF2_ES	$A = \frac{1}{16}$	BDF2_ES	$A = 0$
h_c	h_f	$\|\delta_\phi\|_2$	Rate	$\|\delta_\phi\|_2$	Rate	$\|\delta_\phi\|_2$	Rate
$\frac{3.2}{16}$	$\frac{3.2}{32}$	5.6689×10^{-2}	–	3.7025×10^{-2}	–	3.6712×10^{-2}	–
$\frac{3.2}{32}$	$\frac{3.2}{64}$	1.6071×10^{-2}	1.819	9.0444×10^{-3}	2.0334	8.9422×10^{-3}	2.0375
$\frac{3.2}{64}$	$\frac{3.2}{128}$	4.1541×10^{-3}	1.952	2.2503×10^{-3}	2.0069	2.2232×10^{-3}	2.0080
$\frac{3.2}{128}$	$\frac{3.2}{256}$	1.0472×10^{-3}	1.988	5.6195×10^{-4}	2.0016	5.5504×10^{-4}	2.0019
$\frac{3.2}{256}$	$\frac{3.2}{512}$	(too expensive)	–	1.4044×10^{-4}	2.0005	1.3871×10^{-4}	2.0005

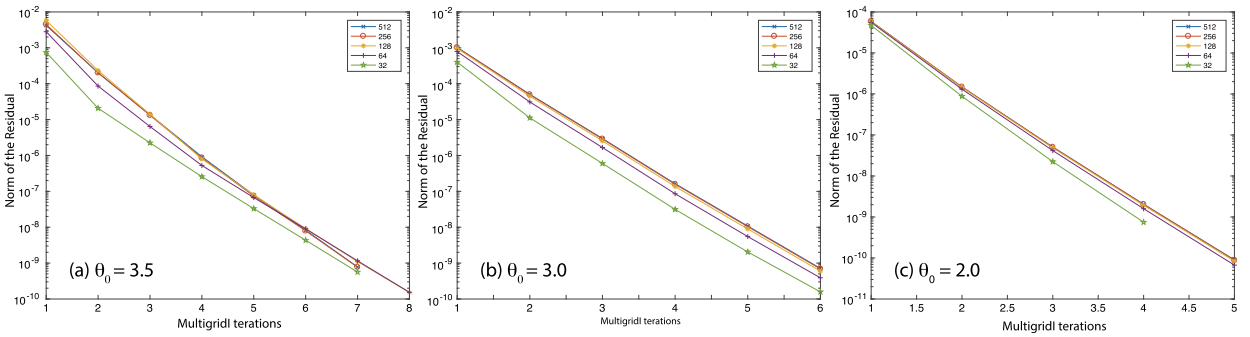

Fig. 2. Solver convergence (complexity) test for the problem defined in Section 7.3. We use a fixed time step size, $\Delta t = 10^{-1}$ for all runs. We plot on a semi-log scale of the residual $\|r^n\|_{\ell^2}$ with respect to the multigrid iteration count n at the 10th and final time step, *i.e.*, $t = T = 1.0$. The initial data is defined in (113), and the other parameters are as follows: $L = L_x = L_y = 3.2$; $\varepsilon = 0.2$; $\mathcal{M} \equiv 1$; $\delta = 10^{-5}$. The quench parameter is varied $\theta_0 = 3.5$, 3.0, and 2.0. The number of multigrid smoothing sweeps is held fixed at $\lambda = 2$. The multigrid stopping tolerance is taken to be $\tau = 10^{-9}$. We observe that the residual is decreasing by a nearly constant factor for each iteration. More iterations are required for larger values of θ_0, as expected.

To compute a rate of convergence, the "Cauchy difference," δ_ϕ, is computed between approximate solutions obtained with successively finer mesh sizes. For details of the test in the cell-centered grid setting, see, for example, [63]. The parameters are (domain size) $L = L_x = L_y = 3.2$; (interfacial parameter) $\varepsilon = 0.2$; (mobility) $\mathcal{M} \equiv 1$; (quench parameter) $\theta_0 = 3.0$; (ln regularization parameter) $\delta = 10^{-5}$; (final time) $T = 0.4$; (solver stopping tolerance) $\tau = 10^{-10}$; (stabilization parameter for BFD2_ES) $A = \frac{1}{16}$ and $A = 0$. The refinement path for the first-order CS1 scheme is quadratic, $\Delta t = 0.4h^2$, and the refinement path for the second-order BDF2_ES scheme is linear, $\Delta t = 0.8h$. The test results, displayed in Table 3, confirm the predicted accuracy: first order in time and second order in space for CS1 and fully second order for the BDF2_CS scheme. When $A = 0$, the BDF2_ES scheme is not provably energy dissipative, but it typically performs well and has a smaller error compared to when $A > 0$. Such an improved numerical accuracy comes from a smaller local truncation error via a direct Taylor expansion. See Table 3.

7.4. Algebraic convergence tests for the multigrid solver

In this next test, we give some evidence that our multigrid solver for the first-order convex-concave decomposition (CS1) scheme has optimal or nearly optimal complexity. The solvers for the other schemes have similar, near-optimal performance. We use the same test as in Section 7.3. The only difference is that for this test, we use a fixed time step size, $\Delta t = 10^{-1}$ for all runs. We plot on a semi-log scale of the residual $\|r^n\|_2$ with respect to the multigrid iteration count n at the 10th and final time step, *i.e.*, $t = T = 1.0$. The initial condition is defined in (113), and the other parameters are as follows: $L = L_x = L_y = 3.2$; $\varepsilon = 0.2$; $\mathcal{M} \equiv 1$; $\delta = 10^{-5}$. The quench parameter is varied, $\theta_0 = 3.5$, 3.0, and 2.0. The number of multigrid smoothing sweeps is held fixed at $\lambda = 2$. The multigrid stopping tolerance is taken to be $\tau = 10^{-9}$. The tests, reported in Fig. 2, indicate that the residual is reduced by nearly the same amount for each multigrid iteration. This is solid evidence for optimal or nearly optimal complexity. We do observe some minor degradation for larger values of θ_0, which is expected, since the problem becomes increasingly stiff for larger values of θ_0. In particular, the potential is approaching the super-singular obstacle potential in this limit.

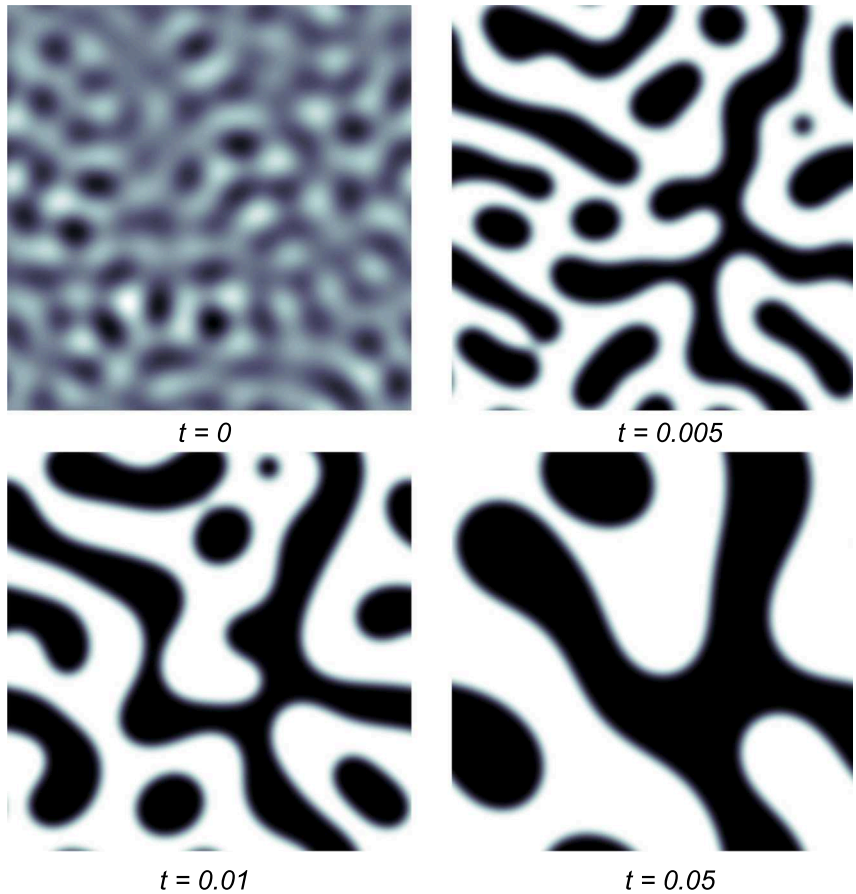

Fig. 3. Initial data and high-resolution approximate solutions at $t = 0.005$, $t = 0.01$, and $t = 0.05$. A high-accuracy solution is computed using the BDF_ES scheme with the stabilization parameter $A = \frac{1}{16}$ and step sizes $\Delta t = 1.0 \times 10^{-6}$, $h = 0.5/512$. The smooth initial data shown in the figure ($t = 0$). The average composition of the solution is $\overline{\phi} = 0.1$, and $-0.1224 \leq \phi(\cdot, t = 0) \leq 0.3162$. The other parameters are $\Omega = (0, 0.5) \times (0, 0.5)$ and $\varepsilon = 5.0 \times 10^{-3}$, $\theta_0 = 3.0$, $\delta = 1.0 \times 10^{-5}$. In the simulation, we observe that, for the high-resolution solution, $0.99750 \geq \phi \geq -0.99856$.

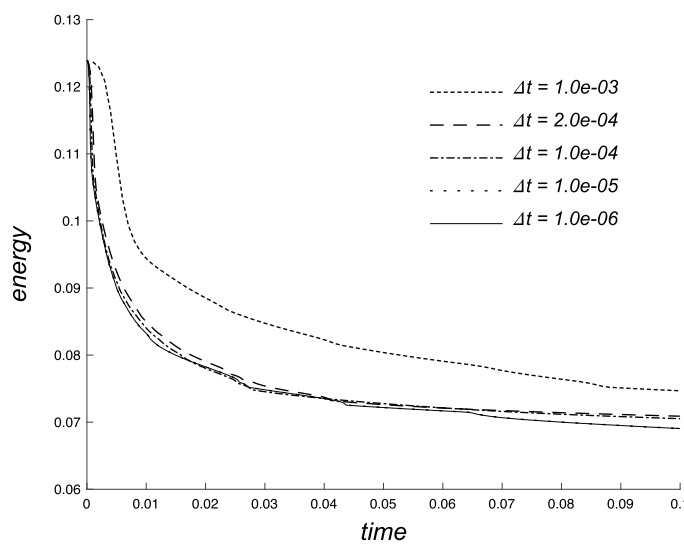

Fig. 4. Energy computations for the simulations represented in Table 2 and Fig. 3. The parameters are given in the captions of Table 2 and Fig. 3. The energy curves for the simulations with $\Delta t = 1.0 \times 10^{-5}$ and $\Delta t = 1.0 \times 10^{-6}$ nearly coincide.

Fig. 5. Initial data and high-resolution approximate solutions at $t = 0.5$ and $t = 1.0$. A high-resolution solution is computed using the BDF2 scheme (105) – (106) with the initial data shown in the figure ($t = 0$). The parameters for the high-resolution approximation are $\Delta t = 1.0 \times 10^{-5}$ and $h = 1.0/256$. The other parameters are $\Omega = (0, 1.0) \times (0, 1.0)$ and $\varepsilon = 5.0 \times 10^{-3}$, $\theta_0 = 3.0$, $\delta = 1.0 \times 10^{-5}$. The average composition of the solution is $\overline{\phi} = 0.2$. Significant coarsening occurs between $t = 0$ and $t = 1.0$. In the simulation, we observe that, for the approximate solution, $0.99672 \geq \phi \geq -0.99821$.

Table 4
The errors, average V-cycle iteration numbers for the FAS multigrid solvers, and the maximum values of ϕ for the various schemes with fixed time and space step sizes $\Delta t = 1.0 \times 10^{-4}$ and $h = 1.0/256$. The other parameters are $\Omega = (0, 1.0) \times (0, 1.0)$ and $\varepsilon = 5.0 \times 10^{-3}$, $\theta = 3.0$, $\delta = 1.0 \times 10^{-5}$. The "errors," which are reported at times $t = 0.1$, $t = 0.5$ and $t = 1.0$, are precisely the differences between the comparison approximations and the high-resolution target approximation computed using the BDF2 with the much smaller time step size $\Delta t = 5 \times 10^{-6}$. See Fig. 5.

Scheme	Error $t = 0.1$	Error $t = 0.5$	Error $t = 1$	Ave. Itr.	$\max_{i,j,k} \phi^k_{i,j}$
BDF2	2.2496e−04	9.3172e−04	5.2566e−04	4.6237	0.99671
BDF2_ES	3.9485e−02	1.9105e−01	2.6703e−01	3.7373	0.99890
BDF2_ES $A = 0$	5.8446e−03	1.9113e−02	1.4204e−02	3.5390	0.99913
BE	2.7285e−03	8.4211e−03	5.7435e−03	6.5645	0.99668
CS1	3.5965e−01	5.6166e−01	7.5356e−01	4.0003	0.99621

Table 5
The errors, average V-cycle iteration numbers for the FAS multigrid solvers, and the maximum values of ϕ for the various scheme with fixed time and space step sizes $\Delta t = 5.0 \times 10^{-5}$ and $h = 1.0/256$. The other parameters are $\Omega = (0, 1.0) \times (0, 1.0)$ and $\varepsilon = 5.0 \times 10^{-3}$, $\theta = 3.0$, $\delta = 1.0 \times 10^{-5}$. The "errors," which are reported at times $t = 0.1$, $t = 0.5$ and $t = 1.0$, are precisely the differences between the comparison approximations and the high-resolution target approximation computed using the BDF2 with the much smaller time step size $\Delta t = 5 \times 10^{-6}$. See Fig. 5.

Scheme	Error $t = 0.1$	Error $t = 0.5$	Error $t = 1$	Ave. Itr.	$\max_{i,j,k} \phi^k_{i,j}$
BDF2	5.7762e−05	2.3749e−04	1.3267e−04	3.49560	0.99671
BDF2_ES	1.0079e−02	1.1464e−02	7.6568e−03	2.70300	0.99668
BDF2_ES $A = 0$	1.6392e−03	5.1465e−03	4.0927e−03	2.6401	0.99671
BE	1.3510e−03	4.1560e−03	2.8182e−03	3.63475	0.99670
CS1	1.4975e−01	2.7690e−01	3.5650e−01	2.78145	0.99628

7.4.1. Initial data and a high-resolution approximate solution at $t = 1$

A high-resolution solution is computed using the BDF2 scheme (105)–(106) with the initial data shown in Fig. 5 ($t = 0$). The parameters for the approximation are $\Delta t = 5 \times 10^{-6}$ and $h = 1.0/256$. The physical parameters are $\Omega = (0, 1)^2$, $\varepsilon = 5.0 \times 10^{-3}$, $\mathcal{M} \equiv 1$; $\theta_0 = 3.0$, and $\delta = 1.0 \times 10^{-5}$. Note that the time step size $\Delta t = 5 \times 10^{-6}$ is 10 times smaller than what will be used in the comparison tests, and we will treat the approximation obtained here as the target solution. We point out that computing the target solution with the slightly larger time step of $\Delta t = 1 \times 10^{-5}$ does not change the results presented in Tables 4 and 5 in any significant way.

7.4.2. Comparison results

For the comparison computations we use the same parameters as above – $h = 1.0/256$, $\Omega = (0, 1)^2$, $\varepsilon = 5.0 \times 10^{-3}$, $\mathcal{M} \equiv 1$; $\theta_0 = 3.0$, $\delta = 1.0 \times 10^{-5}$ – but we use larger time step sizes: $\Delta t = 1.0 \times 10^{-4}$ (Table 4) and $\Delta t = 5.0 \times 10^{-5}$

(Table 5). To solve all these schemes, we employ the FAS multigrid methods detailed above. The results of the tests are reported in Tables 4 and 5, and they paint a complicated picture. The BDF2 scheme shows excellent accuracy and efficiency. Based on our experience, this method is the most accurate of the four that have been test, which is why it is used to generate our target solution. Our new BDF2_ES scheme is slightly more efficient, but not nearly as accurate. When the stabilization parameter is set to zero ($A = 0$), its accuracy increases significantly, but its provable stability is lost.

The first-order convex-concave decomposition scheme is the worst in the tests for accuracy, but the second best in efficiency per step. The worst in efficiency per time step is the backward Euler scheme; like the BDF2 scheme, it does not have a convex structure. But, like pure BDF2, the fully implicit backward Euler has very good accuracy, better than the energy stabilized BDF2 scheme with the stabilization parameter set to zero.

All these schemes are positivity preserving, as long as they are solvable. Even though we did not prove this claim for the fully implicit schemes, such a fact can be established in our theory, though the details are significantly more complicated and are skipped in this presentation.

8. Concluding remarks

In this paper we have presented and analyzed two positivity preserving, energy stable finite difference schemes for the Cahn-Hilliard model with a logarithmic Flory Huggins energy potential, including both the first and second order temporal accuracy. In particular, the singular nature of the logarithmic term around the values of -1 and 1 prevents the numerical solution from reaching these singular values, and this subtle fact indicates that the proposed numerical algorithm has a unique solution with preserved positivity for the logarithmic arguments. In turn, the numerical scheme is always well-defined, as long as the numerical solution stays bounded at the previous time step, which is natural. And also, an unconditional energy stability has been theoretically justified; in particular, an artificial Douglas-Dupont regularization term is added in the second order BDF scheme to ensure the energy stability. In addition, an optimal rate convergence in the $\ell^\infty(0, T; H_h^{-1}) \cap \ell^2(0, T; H_h^1)$ norm has been established for both the first and second order accurate schemes. An efficient multigrid solver is applied in the practical implementation, and some numerical results are presented, which demonstrate the robustness and efficiency of the numerical solver.

Declaration of Competing Interest

There is no competing interest.

Acknowledgement

This work is supported in part by the grants NSFC 11671098, 91630309, a 111 project B08018 (W. Chen), NSF DMS-1418689 (C. Wang), NSF DMS-1715504, NSFC 11871159 and Fudan University start-up (X. Wang) and NSF DMS-1719854 (S. Wise). C. Wang also thanks the Key Laboratory of Mathematics for Nonlinear Sciences, Fudan University, and Shanghai Center for Mathematical Sciences, for support during his visit. During the preparation of the manuscript, S. Wise was partially supported by the Techniche Universität, Dresden (TUD), as a senior Dresden Fellow, and by Oak Ridge National Laboratory (ORNL). S. Wise thanks TUD and Prof. Axel Voigt for the generous support and hospitality and thanks Cory Hauck (ORNL) for support and discussions on this and related topics.

Appendix A. The first order numerical scheme for the Allen-Cahn equation

For the Allen-Cahn equation (2), the first order scheme could be formulated as: given $\phi^n \in \mathcal{C}_{\text{per}}$, find $\phi^{n+1}, \mu^{n+1} \in \mathcal{C}_{\text{per}}$, such that

$$\frac{\phi^{n+1} - \phi^n}{\Delta t} = -\hat{\mathcal{M}}^n \mu^{n+1}, \quad \text{with } \mu^{n+1} \text{ given by (16)}. \tag{114}$$

The mobility approximation is defined as $\hat{\mathcal{M}}^n = \mathcal{M}(\phi^n) \in \mathcal{C}_{\text{per}}$. The positivity-preserving property is stated in the following theorem. Again, we assume that $\mathcal{M}(\phi) \equiv 1$ for simplicity of presentation.

Theorem A.1. *Assume that $\mathcal{M}(\phi) \equiv 1$. Given $\phi^n \in \mathcal{C}_{\text{per}}$, with $\|\phi^n\|_\infty \le M$, for some $M > 0$, there exists a unique solution $\phi^{n+1} \in \mathcal{C}_{\text{per}}$ to (114), with $\|\phi^{n+1}\|_\infty < 1$. Moreover, if the initial data satisfy $\|\phi^0\|_\infty \le 1 - \delta_0$, there exists $\delta^\star \in (0, 1)$, which depends upon δ_0 but is independent of ε and n, so that $\|\phi^n\|_\infty \le 1 - \delta^\star$, $\forall n \in \mathbb{N}$.*

Proof. We observe that, the numerical solution of (114) is equivalent to the minimization of the discrete energy functional

$$\mathcal{J}^n(\phi) := \frac{1}{2\Delta t}\|\phi - \phi^n\|_2^2 + \langle 1 + \phi, \ln(1 + \phi)\rangle_\Omega + \langle 1 - \phi, \ln(1 - \phi)\rangle_\Omega + \frac{\varepsilon^2}{2}\|\nabla_h \phi\|_2^2 - \theta_0 \langle \phi, \phi^n\rangle_\Omega, \tag{115}$$

over the compact, convex admissible set $A_h = \left\{\phi \in \mathcal{C}_{\text{per}} \;\middle|\; \|\phi\|_\infty \le 1\right\} \subset \mathbb{R}^{N^3}$. We observe that $\mathcal{J}^n$ is a strictly convex function over this domain. We wish to prove that there exists a minimizer of $\mathcal{J}^n$ at an interior point of A_h. To this end, consider the following closed domain: for a given $\delta \in (0, 1/2)$,

$$A_{h,\delta} := \left\{\phi \in \mathcal{C}_{\text{per}} \;\middle|\; \|\phi\|_\infty \le 1 - \delta\right\} \subset A_h. \tag{116}$$

Since $A_{h,\delta}$ is a compact and convex set in $\mathbb{R}^{N^3}$, there exists a (not necessarily unique) minimizer of $\mathcal{J}^n$ over $A_{h,\delta}$. The key point of our positivity analysis is that such a minimizer could not occur on the boundary of $A_{h,\delta}$, if δ is small enough.

Assume a minimizer of $\mathcal{J}^n$ over $A_{h,\delta}$, denote it by $\phi^\star$, occurs at a boundary point. There is at least one grid point $\vec{\alpha}_0 = (i_0, j_0, k_0)$ such that $|\phi^\star_{\vec{\alpha}_0}| = 1 - \delta$. First, let us assume, that $\phi^\star_{\vec{\alpha}_0} = \delta - 1$, so that the grid function $\phi^\star$ has a global minimum at $\vec{\alpha}_0$. Since $\mathcal{J}^n$ is smooth over $A_{h,\delta}$, for all $\psi \in \mathcal{C}_{\text{per}}$, the directional derivative is

$$d_s \mathcal{J}^n(\phi^\star + s\psi)|_{s=0} = \left\langle \frac{\phi^\star - \phi^n}{\Delta t} + \ln(1+\phi^\star) - \ln(1-\phi^\star) - \theta_0 \phi^n - \varepsilon^2 \Delta_h \phi^\star, \psi \right\rangle_\Omega.$$

If the direction grid function is of the form $\psi_{i,j,k} = \delta_{i,i_0}\delta_{j,j_0}\delta_{k,k_0}$, where $\delta_{k,\ell}$ denotes the usual Kronecker delta function,

$$\frac{1}{h^3} d_s \mathcal{J}^n(\phi^\star + s\psi)|_{s=0} = \ln\delta - \ln(2-\delta) - \theta_0 \phi^n_{\vec{\alpha}_0} - \varepsilon^2 \Delta_h \phi^\star_{\vec{\alpha}_0} + \frac{\delta - 1 - \phi^n_{\vec{\alpha}_0}}{\Delta t}. \tag{117}$$

Since $\phi^\star$ has a minimum at the grid point $\vec{\alpha}_0 = (i_0, j_0, k_0)$, it follows that

$$\phi^\star_{\vec{\alpha}_0} = -1 + \delta \le \phi^\star_{i,j,k}, \quad \forall\, (i,j,k) \ne \vec{\alpha}_0, \quad \text{and} \quad \Delta_h \phi^\star_{\vec{\alpha}_0} \ge 0. \tag{118}$$

The bound $\left\|\phi^n\right\|_\infty \le M$ and the fact that $\delta \in (0, 1/2)$ imply that

$$\delta - 1 - \phi^n_{\vec{\alpha}_0} \le \delta - 1 + M < M - 1/2. \tag{119}$$

Define the parameters

$$\beta_0 := 2\left(1 + \exp\left\{\theta_0 M + \frac{M - 1/2}{\Delta t}\right\}\right)^{-1}, \quad \beta := \min(1/2, \beta_0).$$

If $\delta \in (0, \beta)$, then

$$\ln\delta - \ln(2-\delta) - \theta_0 \phi^n_{\vec{\alpha}_0} + \frac{\delta - 1 - \phi^n_{\vec{\alpha}_0}}{\Delta t} < 0. \tag{120}$$

Using the estimates (118)–(120) in (117) reveals that, provided $0 < \delta < \beta$,

$$\frac{1}{h^3} d_s \mathcal{J}^n(\phi^\star + s\psi)|_{s=0} < 0. \tag{121}$$

This yields a contradiction that $\mathcal{J}^n$ takes a global minimum at $\phi^\star$ over $A_{h,\delta}$, because the directional derivative at this boundary point is *negative* in a direction pointing into the interior of $A_{h,\delta}$. In other words, going in the direction of ψ, we are certain to find an interior point $\phi^\star + s\psi$, provided $s > 0$ is sufficiently small, such that $\mathcal{J}^n(\phi^\star + s\psi) < \mathcal{J}^n(\phi^\star)$.

Using quite similar arguments, if $\phi^\star_{\vec{\alpha}_0} = 1 - \delta$, and $\delta \in (0, \beta)$, we would find that

$$\frac{1}{h^3} d_s \mathcal{J}^n(\phi^\star + s\psi)|_{s=0} > 0. \tag{122}$$

A combination of these two facts shows that the global minimum of $\mathcal{J}^n$ over $A_{h,\delta}$ could only possibly occur at an interior point, when $\delta \in (0, \beta)$. We conclude that there must be a solution $\phi \in \left(A_{h,\delta}\right)^0$, the interior region of $A_{h,\delta}$, so that for all $\psi \in \mathcal{C}_{\text{per}}$,

$$0 = d_s \mathcal{J}^n(\phi + s\psi)|_{s=0}. \tag{123}$$

which is equivalent to the numerical solution of (114), provided $\delta \in (0, \beta)$. The existence of a "positive" numerical solution is, therefore, established. In addition, since $\mathcal{J}^n$ is a strictly convex function over A_h, the uniqueness analysis for this numerical solution is straightforward.

For the second part of this theorem, let us make the *a priori* assumption that, for some $\delta_0 \in (0, 1)$, $\left\|\phi^0\right\|_\infty = 1 - \delta_0$. Furthermore, choose $\delta_1 \in (0, 1)$ so that

$$\delta_1 < \frac{2}{\exp(\theta_0 + 1)}.$$

Define $\delta^\star = \min(\delta_0, \delta_1)$, and consider the space $A_{h,\delta^\star}$. Suppose that $\phi^{1,\star}$ is the minimizer of J^0 over $A_{h,\delta^\star}$. If we use an analysis similar to that of the first part, we can show that, if $\phi^{1,\star}$ is a boundary point of $A_{h,\delta^\star}$, we obtain a contradiction. Specifically, if at $\vec{\alpha}_0 = (i_0, j_0, k_0)$, $\phi^{\star,1}_{\vec{\alpha}_0} = \delta^\star - 1$ (a minimum point), then we find

$$\begin{aligned} 0 \le & \ln\delta^\star - \ln(2-\delta^\star) - \theta_0\phi^0_{\vec{\alpha}_0} - \varepsilon^2\Delta_h\phi^{1,\star}_{\vec{\alpha}_0} + \frac{\delta^\star - 1 - \phi^0_{\vec{\alpha}_0}}{\Delta t} \\ & \le \ln\delta^\star - \ln(2-\delta^\star) + \theta_0 < 0. \end{aligned}$$

Similarly, if at $\vec{\alpha}_0 = (i_0, j_0, k_0)$, $\phi^{\star,1}_{\vec{\alpha}_0} = 1 - \delta^\star$ (a maximum point), then we likewise discover that $0 > 0$. This implies, ultimately, that the minimizer $\phi^1 \in A_h$ of J^0 satisfies the bound

$$\left\|\phi^1\right\|_\infty < 1 - \delta^\star.$$

Clearly, $\delta^\star$ only depends on δ_0 and θ_0; it is independent of ε. This argument can be continued inductively, and we can conclude that, for any $n \in \mathbb{N}$,

$$\left\|\phi^n\right\|_\infty < 1 - \delta^\star.$$

The proof of Theorem A.1 is complete. □

The analysis for the non-constant mobility case, the unconditional energy stability analysis and the optimal rate convergence estimate follow very similar style as that for the Cahn-Hilliard equation. The details are left to interested readers.

Appendix B. Proof of Theorem 3.1

For any $\phi \in \mathring{\mathcal{C}}_\Omega$, there exists a unique $\psi \in \mathring{\mathcal{C}}_\Omega$ that solves

$$\mathcal{L}_{\check{\mathcal{M}}^n}(\psi) := -\nabla_h \cdot (\check{\mathcal{M}}^n \nabla_h \psi) = \phi. \tag{124}$$

In turn, the following norm may be introduced:

$$\|\phi\|_{\mathcal{L}^{-1}_{\check{\mathcal{M}}^n}} = \sqrt{\left\langle \phi, \mathcal{L}^{-1}_{\check{\mathcal{M}}^n}(\phi)\right\rangle_\Omega}. \tag{125}$$

Similar to Lemma 3.1, the following estimate is needed in the positivity analysis.

Lemma B.1. *Suppose that $\phi_1, \phi_2 \in \mathcal{C}_{\rm per}$, with $\langle \phi_1 - \phi_2, 1\rangle_\Omega = 0$, that is, $\phi_1 - \phi_2 \in \mathring{\mathcal{C}}_{\rm per}$, and assume that $\|\phi_1\|_\infty < 1$, $\|\phi_2\|_\infty \le M$. Then, we have the following estimate:*

$$\left\|\mathcal{L}^{-1}_{\check{\mathcal{M}}^n}(\phi_1 - \phi_2)\right\|_\infty \le C_4 := C_3\mathcal{M}_0^{-1}h^{-1/2}, \tag{126}$$

where $C_3 > 0$ depends only upon M and Ω.

Proof. Define $\psi := \phi_1 - \phi_2$ and $v := \mathcal{L}^{-1}_{\check{\mathcal{M}}^n}(\psi)$. Similar to the estimate (19), we get

$$\|\psi\|_2 = \|\phi_1 - \phi_2\|_2 \le (M+1)|\Omega|^{1/2}. \tag{127}$$

To obtain a bound for $v \in \mathring{\mathcal{C}}_{\rm per}$, observe that, by summation-by-parts,

$$\mathcal{M}_0\|\nabla_h v\|_2^2 \le \left[\check{\mathcal{M}}^n\nabla_h v, \nabla_h v\right]_\Omega = \langle\psi, v\rangle_\Omega \le \|\psi\|_2\cdot\|v\|_2 \le C_{\rm P}\|\psi\|_2\cdot\|\nabla_h v\|_2, \tag{128}$$

in which the discrete Poincaré inequality,

$$\|\psi\|_2 \le C_{\rm P}\|\nabla_h\psi\|_2, \quad \forall\psi \in \mathring{\mathcal{C}}_{\rm per},$$

has been applied in the last step. Therefore

$$\|\nabla_h v\|_2 \le C_{\rm P}\mathcal{M}_0^{-1}\|\psi\|_2. \tag{129}$$

Subsequently, an application of a 3-D inverse inequality, for $v \in \mathring{\mathcal{C}}_{\rm per}$, leads to

$$\begin{aligned} \|v\|_\infty & \le C_{\rm I}h^{-1/2}\|\nabla_h v\|_2 \le C_{\rm I}h^{-1/2}C_{\rm P}\mathcal{M}_0^{-1}\|\psi\|_2 \\ & \le C_{\rm I}h^{-1/2}C_{\rm P}\mathcal{M}_0^{-1}(M+1)|\Omega|^{1/2}, \end{aligned} \tag{130}$$

where the constant in the inverse inequality, $C_{\rm I} > 0$, is independent of h. Therefore, (126) is valid, with $C_3 := C_{\rm I}C_{\rm P}(M+1)|\Omega|^{1/2}$. This completes the proof. □

Then we proceed into the proof of Theorem 3.1.

Proof. The proof of this theorem follows the same ideas as in that of Theorem 2.1; we just provide a brief outline. Similar to (34), the numerical solution of (15) is equivalent to the minimization of the following discrete energy functional:

$$\mathcal{J}^n(\phi) = \frac{1}{2\Delta t}\left\|\phi-\phi^n\right\|^2_{\mathcal{L}^{-1}_{\check{\mathcal{M}}^n}} + \langle 1+\phi, \ln(1+\phi)\rangle_\Omega + \langle 1-\phi, \ln(1-\phi)\rangle_\Omega + \frac{\varepsilon^2}{2}\left\|\nabla_h\phi\right\|_2^2 - \theta_0\left\langle\phi,\phi^n\right\rangle_\Omega, \tag{131}$$

over the admissible set

$$A_h := \left\{\phi\in\mathcal{C}_{\text{per}} \;\middle|\; \|\phi\|_\infty\le 1,\ \left\langle\phi-\overline{\phi}_0, 1\right\rangle_\Omega = 0\right\}.$$

The equivalent minimization problem is similar to previous one: find a minimizer $\varphi\in\mathring{A}_h$ the functional

$$\mathcal{F}^n(\varphi) := \mathcal{J}^n(\varphi+\overline{\phi}_0), \quad \text{with} \quad \mathring{A}_h := \left\{\varphi\in\mathring{\mathcal{C}}_{\text{per}} \;\middle|\; -1-\overline{\phi}_0\le\varphi\le 1-\overline{\phi}_0\right\}\subset\mathbb{R}^{N^3}.$$

There exists a (not necessarily unique) minimizer of $\mathcal{F}^n$ over the restricted set $\mathring{A}_{h,\delta}$, defined in (37), where $\delta\in(0, 1/2)$. To get a contradiction, suppose that the minimizer of $\mathcal{F}^n$, call it $\varphi^\star$, occurs at a boundary point of $\mathring{A}_{h,\delta}$. There is at least one grid point $\vec{\alpha}_0=(i_0, j_0, k_0)$ such that $|\varphi^\star_{\vec{\alpha}_0}+\overline{\phi}_0| = 1-\delta$. As before, we first assume that $\varphi^\star_{\vec{\alpha}_0}+\overline{\phi}_0 = \delta-1$, so that the grid function $\varphi^\star$ has a global minimum at $\vec{\alpha}_0$. Suppose that $\vec{\alpha}_1=(i_1, j_1, k_1)$ is a grid point at which $\varphi^\star$ achieves its maximum.

The directional derivative, in the direction

$$\psi_{i,j,k} = \delta_{i,i_0}\delta_{j,j_0}\delta_{k,k_0} - \delta_{i,i_1}\delta_{j,j_1}\delta_{k,k_1},$$

satisfies

$$\begin{aligned}\frac{1}{h^3}d_s\mathcal{F}^n(\varphi^\star+s\psi)|_{s=0} = {}& \ln(1+\varphi^\star_{\vec{\alpha}_0}+\overline{\phi}_0) - \ln(1-\varphi^\star_{\vec{\alpha}_0}-\overline{\phi}_0) - \ln(1+\varphi^\star_{\vec{\alpha}_1}+\overline{\phi}_0) + \ln(1-\varphi^\star_{\vec{\alpha}_1}-\overline{\phi}_0)\\ & - \theta_0(\phi^n_{\vec{\alpha}_0}-\phi^n_{\vec{\alpha}_1}) - \varepsilon^2(\Delta_h\varphi^\star_{\vec{\alpha}_0}-\Delta_h\varphi^\star_{\vec{\alpha}_1}) + \frac{1}{\Delta t}\mathcal{L}^{-1}_{\check{\mathcal{M}}^n}(\varphi^\star-\phi^n+\overline{\phi}_0)_{\vec{\alpha}_0}\\ & - \frac{1}{\Delta t}\mathcal{L}^{-1}_{\check{\mathcal{M}}^n}(\varphi^\star-\phi^n+\overline{\phi}_0)_{\vec{\alpha}_1}.\end{aligned} \tag{132}$$

We now apply Lemma B.1 to obtain (keeping in mind that $\phi^* = \varphi^* + \bar{\phi}_0$)

$$-2C_4 \le \mathcal{L}^{-1}_{\check{\mathcal{M}}^n}(\phi^\star-\phi^n)_{\vec{\alpha}_0} - \mathcal{L}^{-1}_{\check{\mathcal{M}}^n}(\phi^\star-\phi^n)_{\vec{\alpha}_1} \le 2C_4. \tag{133}$$

This, together with some other estimates, obtained as in the proof of Theorem 2.1, yields

$$\frac{1}{h^3}d_s\mathcal{F}^n(\varphi^\star+s\psi)|_{s=0} \le \ln\frac{\delta}{2-\delta} - \ln\frac{1+\overline{\phi}_0}{1-\overline{\phi}_0} + C_5. \tag{134}$$

where $C_5 := 2M\theta_0 + 2C_4\Delta t^{-1}$. For $\delta\in(0, 1/2)$ sufficiently small, the right hand side is strictly less than 0. The rest of the analysis follows the proof of Theorem 2.1; the details are left to the interested readers. □

Remark B.1. In the proof of Theorem 3.1, the point-wise positivity of the mobility, $\check{\mathcal{M}}^n \ge \mathcal{M}_0 > 0$, is assumed for the convenience of the analysis. However, at the PDE level, the CH flow with a degenerate mobility has been analyzed in [8,32]. The numerical scheme for the degenerate mobility equation will also be considered in the authors' future works. In fact, our assumption could be relaxed to allow for certain mobilities satisfying $\mathcal{M}(\phi^n) > 0$ at a point-wise level; the technical details are left to interested readers. In particular, for the case of the standard symmetric degenerate mobility, $\mathcal{M}(\phi) = (1-\phi)(1+\phi)$, the PDE analyses for which were undertaken by [15,32], our analysis would go through, with the help of a subtle fact that $\mathcal{M}(\phi)$ only degenerates at $\phi=-1$ and 1, combined with the positivity-preserving result at the previous time step.

References

[1] H. Abels, On a diffuse interface model for two-phase flows of viscous, incompressible fluids with matched densities, Arch. Ration. Mech. Anal. 194 (2) (2009) 463–506.

[2] H. Abels, M. Wilke, Convergence to equilibrium for the Cahn-Hilliard equation with a logarithmic free energy, Nonlinear Anal. 67 (2007) 3176–3193.

[3] S.M. Allen, J.W. Cahn, A microscopic theory for antiphase boundary motion and its application to antiphase domain coarsening, Acta Metall. 27 (1979) 1085.

[4] J. Barrett, J. Blowey, An error bound for the finite element approximation of the Cahn-Hilliard equation with logarithmic free energy, Numer. Math. 72 (1995) 1–20.

[5] J. Barrett, J. Blowey, An error bound for the finite element approximation of a model for phase separation of a multi-component alloy, IMA J. Numer. Anal. 16 (1996) 257–287.

[6] J. Barrett, J. Blowey, Finite element approximation of a model for phase separation of a multi-component alloy with non-smooth free energy, Numer. Math. 77 (1997) 1–34.
[7] J. Barrett, J. Blowey, Finite element approximation of a model for phase separation of a multi-component alloy with a concentration-dependent mobility matrix, IMA J. Numer. Anal. 18 (1998) 287–328.
[8] J. Barrett, J. Blowey, Finite element approximation of the Cahn-Hilliard equation with concentration dependent mobility, Math. Comput. 68 (1999) 487–517.
[9] J. Barrett, J. Blowey, An improved error bound for a finite element approximation of a model for phase separation of a multi-component alloy with a concentration dependent mobility matrix, Numer. Math. 88 (2001) 255–297.
[10] A. Baskaran, Z. Hu, J. Lowengrub, C. Wang, S.M. Wise, P. Zhou, Energy stable and efficient finite-difference nonlinear multigrid schemes for the modified phase field crystal equation, J. Comput. Phys. 250 (2013) 270–292.
[11] A. Baskaran, J. Lowengrub, C. Wang, S. Wise, Convergence analysis of a second order convex splitting scheme for the modified phase field crystal equation, SIAM J. Numer. Anal. 51 (2013) 2851–2873.
[12] J.F. Blowey, M.I.M. Copetti, C.M. Elliott, Numerical analysis of a model for phase separation of a multi-component alloy, IMA J. Numer. Anal. 16 (1996) 111–139.
[13] J.F. Blowey, C.M. Elliott, The Cahn-Hilliard gradient theory for phase separation with non-smooth free energy. Part I: mathematical analysis, Eur. J. Appl. Math. 2 (1991) 233–279.
[14] J.F. Blowey, C.M. Elliott, The Cahn-Hilliard gradient theory for phase separation with non-smooth free energy. Part II: numerical analysis, Eur. J. Appl. Math. 3 (1992) 147–179.
[15] J.W. Cahn, C.M. Elliott, A. Novick-Cohen, The Cahn-Hilliard equation with a concentration dependent mobility: motion by minus the Laplacian of the mean curvature, Eur. J. Appl. Math. 7 (1996) 287–301.
[16] J.W. Cahn, J.E. Hilliard, Free energy of a nonuniform system. I. Interfacial free energy, J. Chem. Phys. 28 (1958) 258–267.
[17] W. Chen, S. Conde, C. Wang, X. Wang, S.M. Wise, A linear energy stable scheme for a thin film model without slope selection, J. Sci. Comput. 52 (2012) 546–562.
[18] W. Chen, Y. Liu, C. Wang, S.M. Wise, An optimal-rate convergence analysis of a fully discrete finite difference scheme for Cahn-Hilliard-Hele-Shaw equation, Math. Comput. 85 (2016) 2231–2257.
[19] W. Chen, C. Wang, X. Wang, S.M. Wise, A linear iteration algorithm for energy stable second order scheme for a thin film model without slope selection, J. Sci. Comput. 59 (2014) 574–601.
[20] K. Cheng, W. Feng, C. Wang, S.M. Wise, An energy stable fourth order finite difference scheme for the Cahn-Hilliard equation, J. Comput. Appl. Math. (2018), https://doi.org/10.1016/j.cam.2018.05.039, in press.
[21] K. Cheng, Z. Qiao, C. Wang, A third order exponential time differencing numerical scheme for no-slope-selection epitaxial thin film model with energy stability, J. Sci. Comput. (2018), submitted for publication: https://arxiv.org/abs/1903.03296.
[22] L. Cherfils, A. Miranville, S. Zelik, The Cahn-Hilliard equation with logarithmic potentials, Milan J. Math. 79 (2011) 561–596.
[23] A. Christlieb, J. Jones, K. Promislow, B. Wetton, M. Willoughby, High accuracy solutions to energy gradient flows from material science models, J. Comput. Phys. 257 (2014) 193–215.
[24] M.I.M. Copetti, C.M. Elliott, Numerical analysis of the Cahn-Hilliard equation with a logarithmic free energy, Numer. Math. 63 (1992) 39–65.
[25] J. Cummings, J.S. Lowengrub, B.G. Sumpter, S.M. Wise, R. Kumar, Modeling solvent evaporation during thin film formation in phase separating polymer mixtures, Soft Matter 14 (2018) 1833–1846.
[26] A. Debussche, L. Dettori, On the Cahn-Hilliard equation with a logarithmic free energy, Nonlinear Anal. 24 (1995) 1491–1514.
[27] A. Diegel, X. Feng, S.M. Wise, Convergence analysis of an unconditionally stable method for a Cahn-Hilliard-Stokes system of equations, SIAM J. Numer. Anal. 53 (2015) 127–152.
[28] A. Diegel, C. Wang, X. Wang, S.M. Wise, Convergence analysis and error estimates for a second order accurate finite element method for the Cahn-Hilliard-Navier-Stokes system, Numer. Math. 137 (2017) 495–534.
[29] A. Diegel, C. Wang, S.M. Wise, Stability and convergence of a second order mixed finite element method for the Cahn-Hilliard equation, IMA J. Numer. Anal. 36 (2016) 1867–1897.
[30] M. Doi, Soft Matter Physics, Oxford University Press, Oxford, UK, 2013.
[31] Q. Du, R. Nicolaides, Numerical analysis of a continuum model of a phase transition, SIAM J. Numer. Anal. 28 (1991) 1310–1322.
[32] C.M. Elliott, H. Garcke, On the Cahn-Hilliard equation with degenerate mobility, SIAM J. Math. Anal. 27 (1996) 404.
[33] C.M. Elliott, A.M. Stuart, The global dynamics of discrete semilinear parabolic equations, SIAM J. Numer. Anal. 30 (1993) 1622–1663.
[34] D. Eyre, Unconditionally gradient stable time marching the Cahn-Hilliard equation, in: J.W. Bullard, R. Kalia, M. Stoneham, L.Q. Chen (Eds.), Computational and Mathematical Models of Microstructural Evolution, vol. 53, Materials Research Society, Warrendale, PA, USA, 1998, pp. 1686–1712.
[35] X. Fan, J. Kou, Z. Qiao, S. Sun, A componentwise convex splitting scheme for diffuse interface models with van der Waals and Peng-Robinson equations of state, SIAM J. Sci. Comput. 39 (2017) B1–B28.
[36] X. Feng, S.M. Wise, Analysis of a fully discrete finite element approximation of a Darcy-Cahn-Hilliard diffuse interface model for the Hele-Shaw flow, SIAM J. Numer. Anal. 50 (2012) 1320–1343.
[37] D. Furihata, A stable and conservative finite difference scheme for the Cahn-Hilliard equation, Numer. Math. 87 (2001) 675–699.
[38] A. Giorgini, M. Grasselli, A. Miranville, The Cahn-Hiliard-Ono equation with singular potential, Math. Models Methods Appl. Sci. 27 (2017) 2485–2510.
[39] A. Giorgini, M. Grasselli, H. Wu, The Cahn-Hilliard-Hele-Shaw system with singular potential, Ann. Inst. Henri Poincaré, Anal. Non Linéaire 35 (2018) 1079–1118.
[40] C. Gräser, R. Kornhuber, U. Sack, Nonsmooth Schur-Newton methods for multicomponent Cahn-Hilliard systems, IMA J. Numer. Anal. 35 (2015) 652–679.
[41] Z. Guan, J.S. Lowengrub, C. Wang, S.M. Wise, Second-order convex splitting schemes for nonlocal Cahn-Hilliard and Allen-Cahn equations, J. Comput. Phys. 277 (2014) 48–71.
[42] Z. Guan, C. Wang, S.M. Wise, A convergent convex splitting scheme for the periodic nonlocal Cahn-Hilliard equation, Numer. Math. 128 (2014) 377–406.
[43] F. Guillén-González, G. Tierra, Second order schemes and time-step adaptivity for Allen-Cahn and Cahn-Hilliard models, Comput. Math. Appl. 68 (8) (2014) 821–846.
[44] J. Guo, C. Wang, S.M. Wise, X. Yue, An H^2 convergence of a second-order convex-splitting, finite difference scheme for the three-dimensional Cahn-Hilliard equation, Commun. Math. Sci. 14 (2016) 489–515.
[45] D. Han, X. Wang, A second order in time, uniquely solvable, unconditionally stable numerical scheme for Cahn-Hilliard-Navier-Stokes equation, J. Comput. Phys. 290 (2015) 139–156.
[46] Z. Hu, S.M. Wise, C. Wang, J. Lowengrub, Stable and efficient finite-difference nonlinear-multigrid schemes for the phase-field crystal equation, J. Comput. Phys. 228 (2009) 5323–5339.
[47] D. Jeong, J. Kim, A practical numerical scheme for the ternary Cahn-Hilliard system with a logarithmic free energy, Physica A 442 (2016) 510–522.
[48] D. Jeong, S. Lee, J. Kim, An efficient numerical method for evolving microstructures with strong elastic inhomogeneity, Model. Simul. Mater. Sci. Eng. 23 (2015) 045007.

[49] D. Li, Z. Qiao, On second order semi-implicit Fourier spectral methods for 2D Cahn-Hilliard equations, J. Sci. Comput. 70 (2017) 301–341.
[50] D. Li, Z. Qiao, T. Tang, Characterizing the stabilization size for semi-implicit Fourier-spectral method to phase field equations, SIAM J. Numer. Anal. 54 (2016) 1653–1681.
[51] Q. Peng, H. Li, Z. Xu, Energy stable linear schemes for the mass-conserved gradient flow with Peng-Robinson equation of state, East Asian J. Appl. Math. 9 (2019) 212–232.
[52] X. Li, Z. Qiao, H. Zhang, An unconditionally energy stable finite difference scheme for a stochastic Cahn-Hilliard equation, Sci. China Math. 59 (2016) 1815–1834.
[53] Y. Liu, W. Chen, C. Wang, S.M. Wise, Error analysis of a mixed finite element method for a Cahn-Hilliard-Hele-Shaw system, Numer. Math. 135 (2017) 679–709.
[54] A. Miranville, On a phase-field model with a logarithmic nonlinearity, Appl. Math. 57 (2012) 215–229.
[55] A. Miranville, S. Zelik, Robust exponential attractors for Cahn-Hilliard type equations with singular potentials, Math. Methods Appl. Sci. 27 (2004) 545–582.
[56] Q. Peng, A convex-splitting scheme for a diffuse interface model with Peng-Robinson equation of state, Adv. Appl. Math. Mech. 9 (5) (2018) 1162–1188.
[57] Q. Peng, Z. Qiao, S. Sun, Stability and convergence analysis of second-order schemes for a diffuse interface model with Peng-Robinson equation of state, J. Comput. Math. 35 (6) (2017) 737–765.
[58] Z. Qiao, S. Sun, Two-phase fluid simulation using a diffuse interface model with Peng-Robinson equation of state, SIAM J. Sci. Comput. 36 (2014) B708–B728.
[59] J. Shen, C. Wang, X. Wang, S.M. Wise, Second-order convex splitting schemes for gradient flows with Ehrlich-Schwoebel type energy: application to thin film epitaxy, SIAM J. Numer. Anal. 50 (2012) 105–125.
[60] U. Trottenberg, C.W. Oosterlee, A. Schüller, Multigrid, Academic Press, New York, 2001.
[61] C. Wang, X. Wang, S.M. Wise, Unconditionally stable schemes for equations of thin film epitaxy, Discrete Contin. Dyn. Syst., Ser. A 28 (2010) 405–423.
[62] C. Wang, S.M. Wise, An energy stable and convergent finite-difference scheme for the modified phase field crystal equation, SIAM J. Numer. Anal. 49 (2011) 945–969.
[63] S.M. Wise, Unconditionally stable finite difference, nonlinear multigrid simulation of the Cahn-Hilliard-Hele-Shaw system of equations, J. Sci. Comput. 44 (2010) 38–68.
[64] S.M. Wise, C. Wang, J.S. Lowengrub, An energy stable and convergent finite-difference scheme for the phase field crystal equation, SIAM J. Numer. Anal. 47 (2009) 2269–2288.
[65] X. Wu, G.J. van Zwieten, K.G. van der Zee, Stabilized second-order convex splitting schemes for Cahn-Hilliard models with application to diffuse-interface tumor-growth models, Int. J. Numer. Methods Biomed. Eng. 30 (2014) 180–203.
[66] Y. Yan, W. Chen, C. Wang, S.M. Wise, A second-order energy stable BDF numerical scheme for the Cahn-Hilliard equation, Commun. Comput. Phys. 23 (2018) 572–602.
[67] X. Yang, J. Zhao, On linear and unconditionally energy stable algorithms for variable mobility Cahn-Hilliard type equation with logarithmic Flory-Huggins potential, Commun. Comput. Phys. 25 (2019) 703–728.